We are IntechOpen,
the world's leading publisher of
Open Access books
Built by scientists, for scientists

**4,800**
Open access books available

**122,000**
International authors and editors

**135M**
Downloads

Our authors are among the

**154**
Countries delivered to

**TOP 1%**
most cited scientists

**12.2%**
Contributors from top 500 universities

CLARIVATE ANALYTICS
**BOOK CITATION INDEX**
INDEXED

**WEB OF SCIENCE**™

Selection of our books indexed in the Book Citation Index
in Web of Science™ Core Collection (BKCI)

Interested in publishing with us?
Contact book.department@intechopen.com

Numbers displayed above are based on latest data collected.
For more information visit www.intechopen.com

**1**

# Applications of CFD in Natural Gas Processing and Transportation

Majid Abedinzadegan Abdi[1], Esam Jassim,
Mohammad Haghighi and Yuri Muzychka
*[1]Memorial University of Newfoundland, St. John's, Newfoundland and Labrador,
Canada*

## 1. Introduction

In this chapter, two examples of CFD applications in natural gas processing and transportation are presented. A commercial software package (Fluent) was used in these studies. The purpose of the studies is briefly discussed, the methodology outlined and boundary conditions and problem specifications are concisely described for each case. The results of investigations and comparisons with experimental tests and literature data are presented to demonstrate how CFD can be applied to practical situations.

## 2. Flow of real gas in supersonic nozzles

The demand for natural gas has encouraged the energy industry toward the discovery of remote offshore reservoirs. Consequently new technologies have to be developed to efficiently produce and transport natural gas to consumption centers. Common design challenges in all gas processing methods for offshore applications are the compactness and reliability of process equipment. Supersonic nozzles have been introduced as an alternative to treat natural gas for offshore applications and to meet the offshore requirements (Hengwei et al. 2005, Alfyorov et al. 2005, Okimoto et al., 2002, Karimi & Abedinzadegan Abdi, 2006, Brouwer & Epsom, 2003). In a supersonic separator the gas temperature is lowered based on the principle of gas expansion where no refrigerant is needed. The compact design of supersonic nozzles is a major advantage over traditional means of natural gas treating technologies particularly for offshore applications. The gas speed in this device is very high preventing fouling or deposition of solids and ice. Refrigeration is self-induced therefore no heat is transferred through the walls and unlike external refrigeration systems, no inhibitor injection and inhibitor recovery system are necessary. Intensive water dew points down to -50 to -60 ºC can be achieved without any cryogenic cooling or use of solid adsorption techniques.

### 2.1 Problem description

Application of CFD technique is demonstrated to predict the behaviour of high pressure natural gas flowing through supersonic nozzles. Supersonic nozzles were selected as it was noticed that there was a potential for these nozzles for applications in natural gas processing industries and very few simulation analysis had been published in the open literature. The

nozzle considered here is a de Laval geometry composed of two sections: the convergent section (subsonic zone) and the divergent section (supersonic zone). However, we also address two other de Laval modified geometries, which are of interest in solid/liquid particles separation; namely throat section (critical zone) with extended constant area throat, and throat section with extended U-shape throat.

The function of the convergent part is to keep the flow uniform and parallel as well as to accelerate the gas. Within the converging section leading to the throat area, the gas is accelerated so that the sonic velocity is reached at the throat and the convergent curvature keeps the gradient in velocity of the flow uniform. In practical conditions, in order to get the sonic speed at the throat, it is required that the inlet diameter is kept larger than $\sqrt{5}$ of the throat diameter (Man et al., 1997) although in some cases the ratio of inlet to throat diameter is apparently less (Arina, 2004).

When the gas reaches the throat, the divergent part of the nozzle can further accelerate the flow depending on the outlet condition. This results in a decrease in pressure and temperature as well as increase in gas velocity. It is likely that under certain conditions the flow cannot expand isentropically to the exit pressure; therefore, an irreversible discontinuity, called a shockwave, can occur.

The shockwave is an abrupt disturbance that causes discontinuous and irreversible changes in fluid properties, such as speed (changing from supersonic to subsonic), pressure, temperature, and density. As a result of the gradients in temperature and velocity that are created by the shock, heat is transferred and energy is dissipated within the gas. These processes are thermodynamically irreversible. As the shock thickness is very small, the cross sectional areas at the upstream and downstream of the shock are considered equal and the energy or heat loss is negligible. The shock can also interact with the boundary layer and this can delay the transition from supersonic flow to subsonic flow even further. The increase of pressure across a shock is an indication of the shock strength that can lead to a sound wave considered as a shockwave of minimum strength.

## 2.2 Basis of CFD simulation

The geometry was modeled using two-dimensional axisymmetric grids. The total pressure and temperature for fully developed turbulent flow were imposed at the nozzle inlet, and no-slip condition was applied at wall boundaries. At the exit plane, ambient pressure and temperature were identified. CFD calculations were carried out using SIMPLEC algorithm and the central differencing scheme.

For turbulent flow model, the k-ε model was used here due to its frequent use for industrial applications, its relative accuracy, and its incorporation in most commercial CFD codes (Pope, 2000).

## 2.3 Results and discussions
### 2.3.1 de *Laval nozzles*

Since most of published research has been concerned with the Laval nozzle, we validated our results by applying the numerical technique for such geometry and compared our results with the most recent available data (Arina, 2004; and Molleson & Stasenko, 2005) before proceeding and applying it to the modified nozzle systems.

Molleson and Stasenko (2005) performed their investigation for a nozzle whose geometry is shown in Figure 1-a. Their working fluid was methane at 70 bar inlet stagnation pressure

and 250 K inlet stagnation temperature while the value of exit Mach number according to their supersonic exit radii was 1.2. The SRK EOS model was used in their study. We used the same geometry and conditions in comparison of the sonic condition and in studying of the effect of a real gas model on the sonic position; MBWR was used as the thermodynamic model.
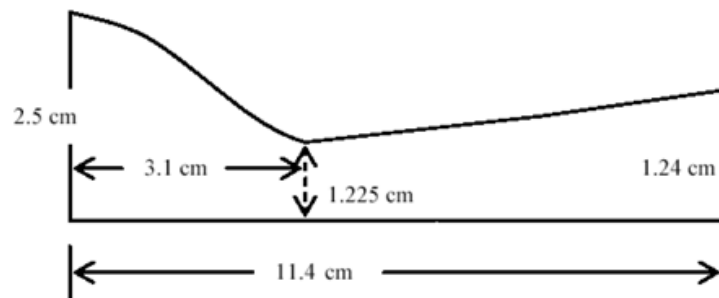


(a) (Molleson et al., 2005)
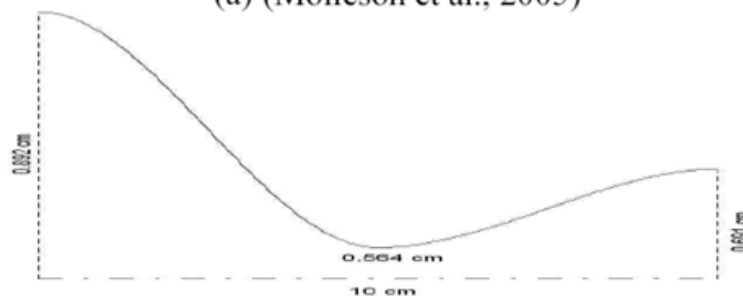


(b) (Arina, 2004)
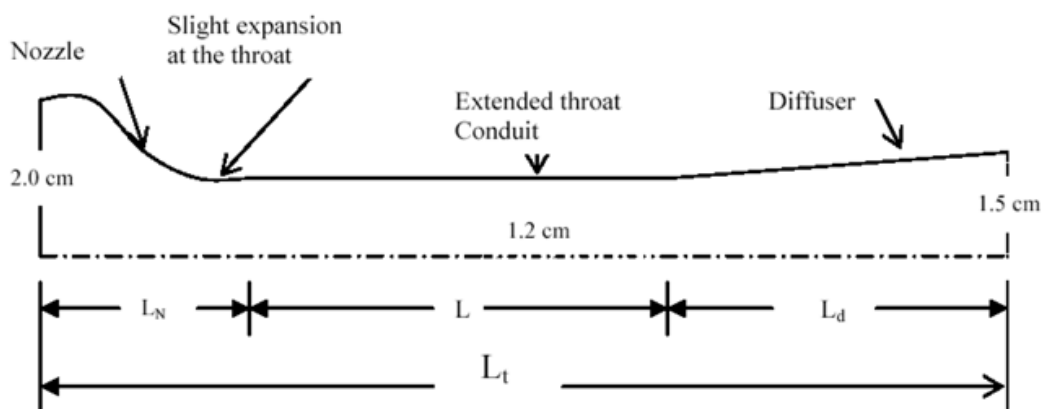


(c) System configuration for long-neck (long constant area/extended throat) Laval nozzle

Fig. 1. Nozzle geometries studied in the research

Figure 2 shows the variation of Mach number with position in real case and the comparison with results obtained from the work of Molleson and Stasenko (2005). One can see that choke (sonic velocity, M=1) occurs at the throat regardless of the EOS used. Also, our results are in very good agreement with their results. The second comparison was performed to

validate our simulation on capturing shockwave position. The comparison is done with recent available data (Arina, 2004). The geometry used in the comparison, shown in Figure 1-b, is adopted from Arina's work (2004). The working fluid was $CO_2$. The dimensions of the assumed Laval-nozzle are:

$$A(x) = 2.5 + 3\left(\frac{x}{x_{th}} - 1.5\right)\left(\frac{x}{x_{th}}\right)^2 \quad \text{for} \quad x \leq x_{th},$$ (1)

$$A(x) = 3.5 - \frac{x}{x_{th}}\left(6 - 4.5\frac{x}{x_{th}} + \left(\frac{x}{x_{th}}\right)^2\right) \quad \text{for} \quad x \geq x_{th}.$$ (2)

Where, $A_{throat} = 1$ $cm^2$, length= 10 $cm$ and the throat placed at $x_{th} = 5$ $cm$.
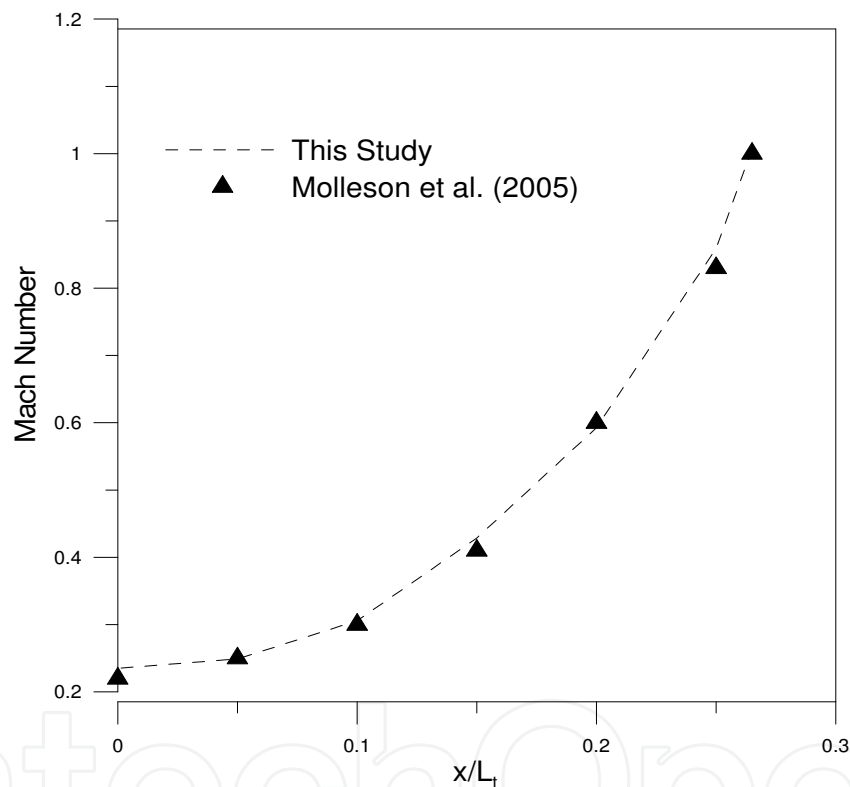


Fig. 2. Comparison of Mach numbers upstream of choke region in the Laval nozzle

Since Arina's simulation was performed near $CO_2$ condensation conditions, for which $T= 1.001T_c$ and $\rho = \rho_c$, we compared our results for a perfect gas case as the FLUENT real gas basis could not predict multiphase conditions. The exit pressure was 83% of the inlet pressure. Our numerical results displayed the same behaviour when similar conditions and working fluids were applied as seen in Figure 3.

2.3.1.1 Real gas vs. Ideal gas assumption

The significance of using real gas models can be more clearly shown when comparison of the location of the shockwave within the Laval nozzle is made for two different gases: methane and nitrogen. At high pressures, the former compressibility factor significantly changes whereas the compressibility for the latter has almost the equivalent value of perfect gases.
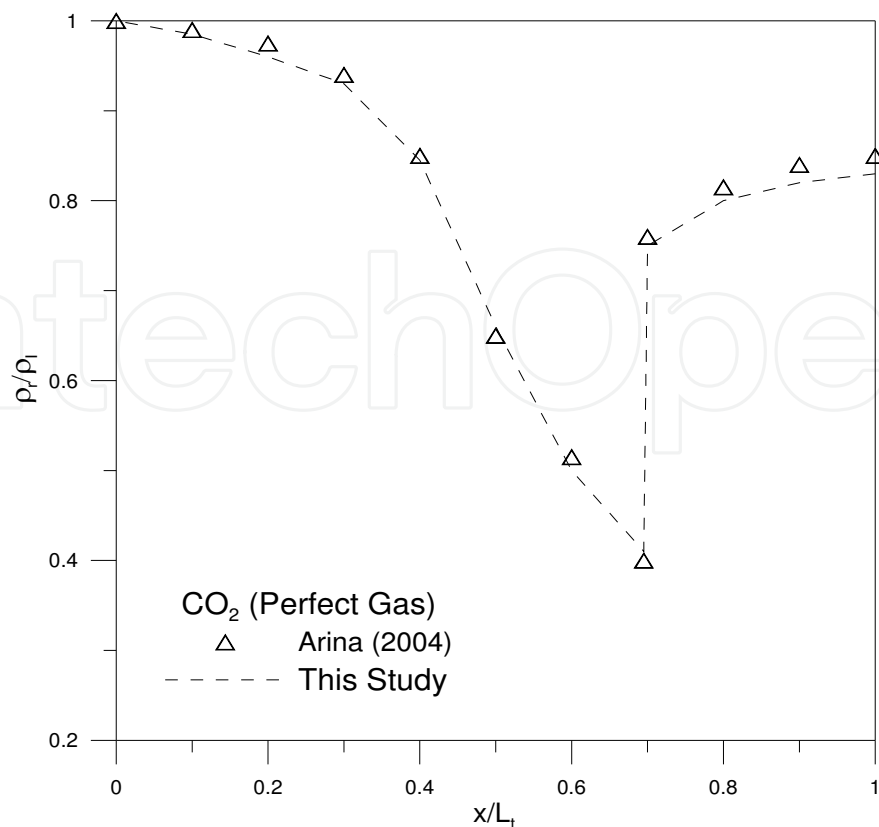
Fig. 3. Comparison of density ratios in the Laval nozzle under perfect gas conditions

2.3.1.2 Shockwave location

The real gas model predicts the shockwave location earlier than the ideal gas model for both gases. However, the differential distance between the ideal and real shock positions is different. In fact, when the ideal gas model is used, shock occurs earlier for nitrogen, see Figure 4-a. On the contrary, the real gas model predicts an opposite behaviour as shown in Figure 4-b. This example proves very clearly that ignoring the real gas effects can obviously lead to misleading results.

2.3.1.3 Real gas effects for a different configuration

The new configuration of the nozzle system designed for natural gas application consists of three different parts: an inlet nozzle (converging part ending to a throat and a slight expansion), diffuser (diverging part, gas final expansion and exit), and a conduit with constant area between these two parts. This latter part does not exist in conventional Laval nozzles where the diffuser or diverging part starts right after the throat and continues uniformly right up to the exit point. The description of the new system is shown in Figure 1-c.

Boundary conditions were chosen in such a way that the inlet pressure was predicted. Hence, we chose mass flow rate and temperature as the inlet boundary conditions while pressure and temperature were chosen for outlet boundary conditions. The working fluid was pure methane, mass flow rate was 430 kg/minute, stagnation temperature at the inlet and outlet were 293 and 280 K, respectively and the stagnation pressure at the outlet was assumed 7 MPa. The stagnation pressure at the inlet was to be predicted. The results of simulation are discussed as follows:
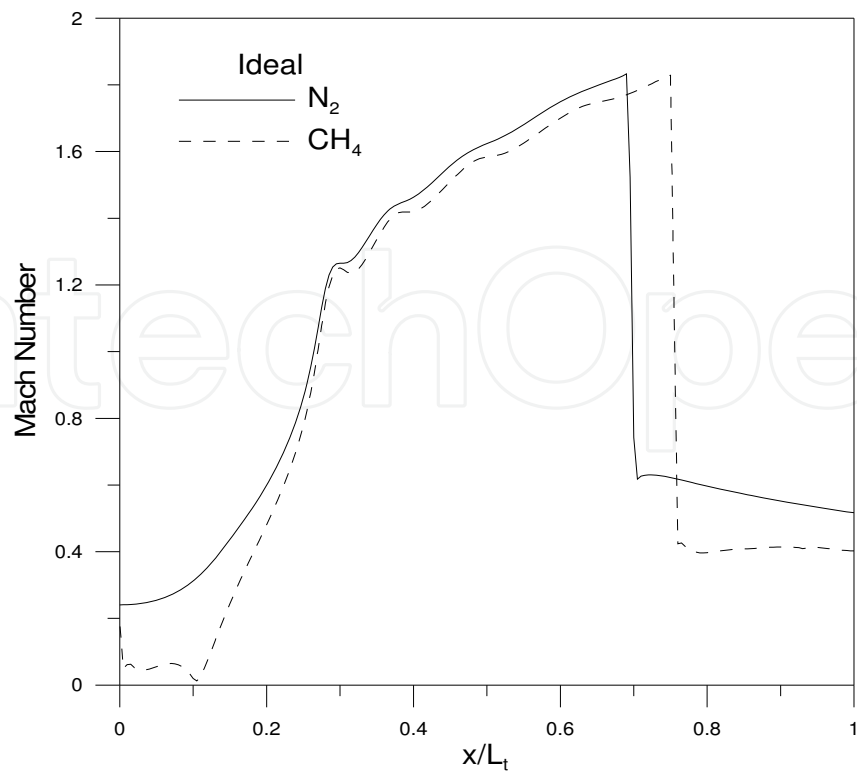
(a)
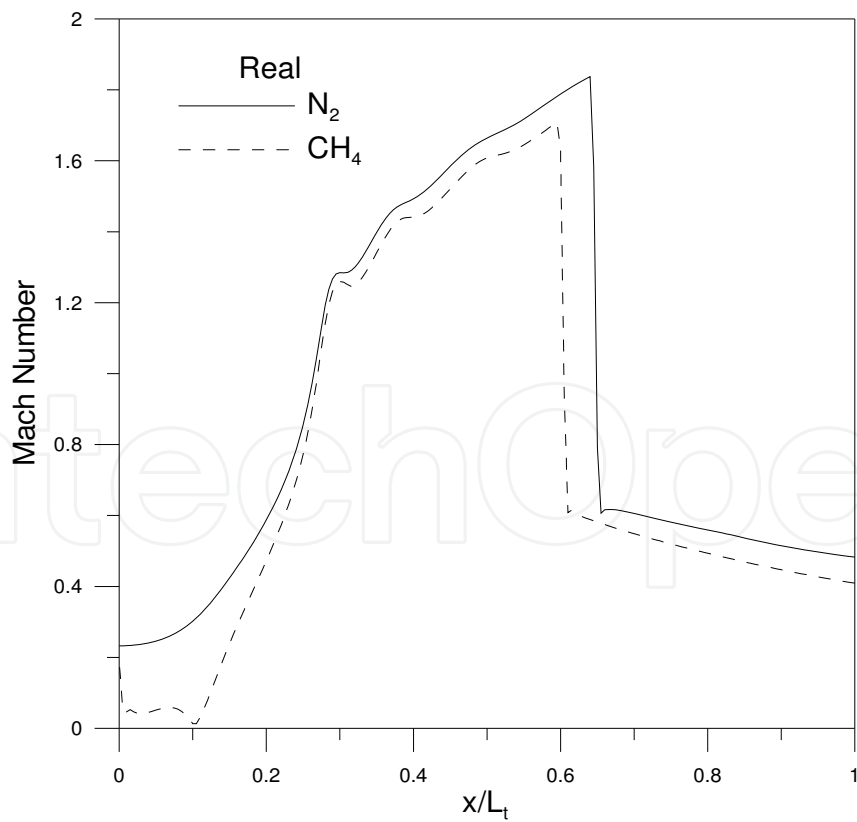


(b)

Fig. 4. Comparison of shock position for nitrogen and methane under (a) ideal and (b) real gas conditions

**Density.** By looking at any fluid textbook, one can see that the conservation of momentum equation directly or indirectly contains density terms in each component. Thus, flow structure is severely affected by any deviation in density calculation. To realize how this deviation will affect the predictions in the nozzle, a graph of the density ratio (real/ideal) along the nozzle system is plotted (see Figure 5). It is evident how erroneous the results might get if the perfect gas model is used, particularly in the vicinity of the shockwave. A large spike of density variations is seen close to the shockwave.
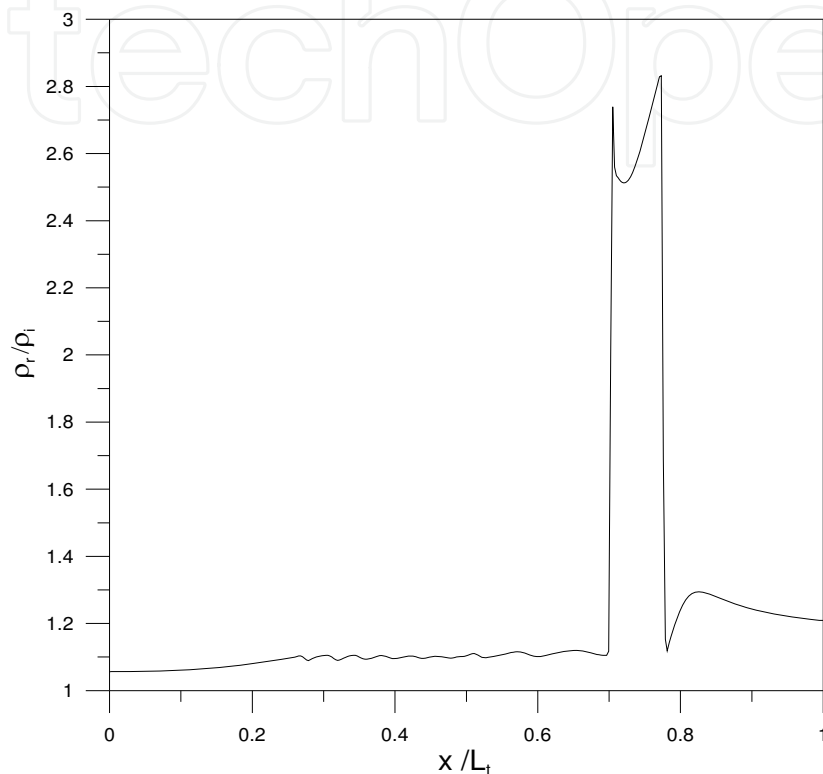


Fig. 5. Centerline density ratio for real gas (methane) simulation in an extended throat nozzle

**Inlet Pressure.** As mentioned earlier, our numerical solution predicts the inlet pressure for the given mass flow rate, outlet pressure and outlet temperature. Figure 6 represents static pressure distribution at the axis. One can see that a significant difference between the real and perfect gas at the inlet pressure is obtained. The real gas model predicts lower required inlet pressure for a given mass flow rate. Thus, better pressure recovery may be obtained. The real gas simulation predicts pressure recoveries in excess of 10% over those predicted by the perfect gas model. Also, the difference between real and ideal static pressures forces the calculation of total pressure to diverge. The errors in evaluating the total pressure and temperature can lead to incorrect predictions for friction loss, work and heat transfer. The differences between the predictions of ideal and real gas models for total pressure and total temperature are considerable. These discrepancies can result in incorrect values for friction losses and other calculated parameters.

**Temperature.** Static temperature decreases during the isentropic expansion process. Figure 7 illustrates the longitudinal variation of static temperature along the insulated wall. It is clearly shown that the temperature reduction in the real gas case is larger than the ideal case. Thus, ideal gas simulation can lead to erroneous results in predicting the potential phase change.
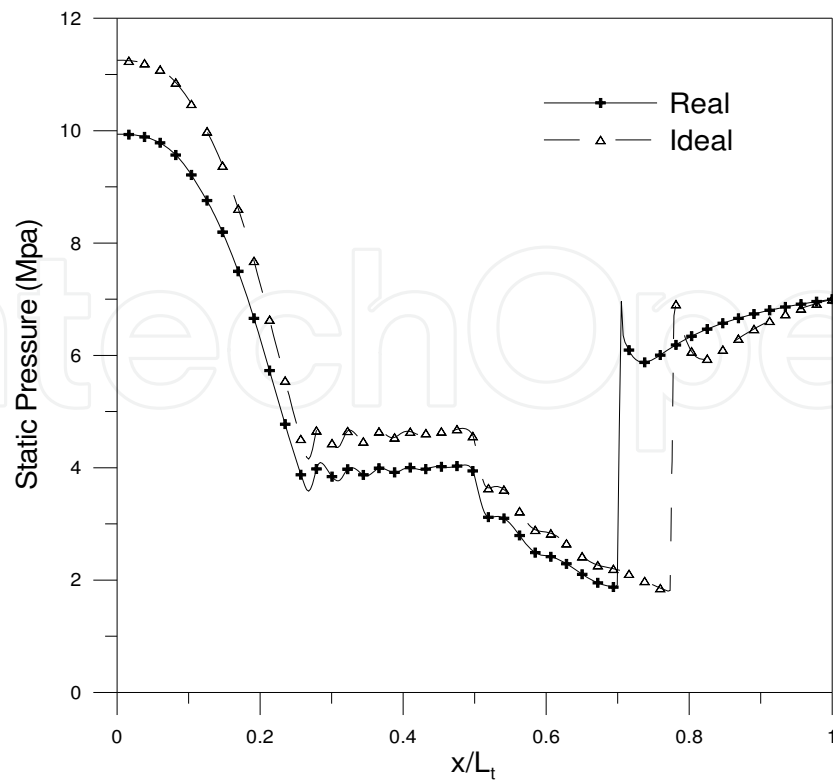
Fig. 6. Centerline static pressure for real gas (methane) simulation in an extended throat nozzle
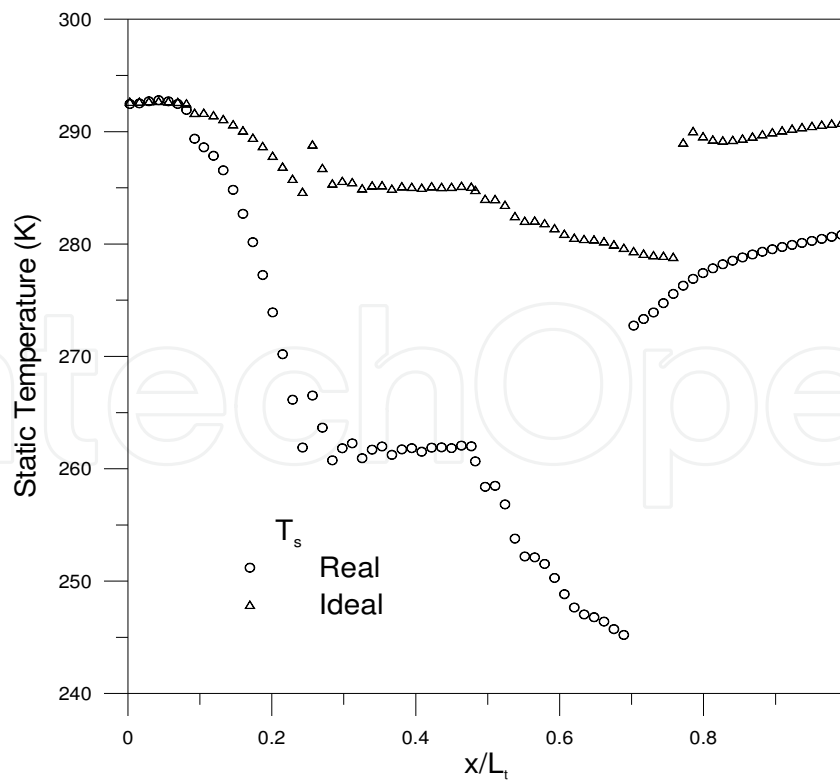


Fig. 7. Wall static temperature distribution for real gas (methane) simulation in an extended throat nozzle

Theoretically, stagnation temperature should retain its value across the shock when the nozzle is insulated. Such conclusion is true when perfect gas law is used as the thermodynamic model. However, the real gas model predicts different conditions in which the stagnation temperature may vary. Stagnation temperature in the real gas case varies across the shock because the specific heat is now varied across the shock as well. Thus, for adiabatic process;

$$\int_{T_{01}}^{T_{02}} Cp(T_0).dT_0 = 0 \tag{3}$$

This means that $T_{02} \neq T_{01}$ across the shockwave.

As a conclusion of modelling of supersonic nozzles using real gas models and discussion of the effect of real gas on the flow of natural gas through these nozzles, the choice of thermodynamic model can substantially affect the modelling results. This includes the position of shockwave, the fluid properties and conditions after the shock, and the work/heat transferred across the system.

### 2.3.2 de *Laval nozzles* with extended straight throat

In this section the influence of geometry on the flow of natural gas through the supersonic nozzle is presented. As mentioned in Section 2.3.1, the nozzle is composed of three sections: the convergent section (subsonic zone), the extended throat section (critical zone) and the divergent section (supersonic zone).

The governing equations are derived from the basic conservation laws including mass (continuity), momentum, and the first and second laws of thermodynamics and the use of a quite suitable real gas Equation of State (EOS).

2.3.2.1 Geometry Influence

**Choke location:** The flow reaches sonic condition at the throat, expands in the slight diverging/expansion section of the nozzle (~ 0.04 $m$), passes through the constant cross-section area, and finally moves across the diffuser within which the shock occurs. The flow downstream of the shock is subsonic. Thus a pressure recovery occurs. The base Fluent simulation cannot predict any phase change therefore it is assumed that no condensation will occur as the gas passes through the nozzle. Gas dynamics parameters for real and ideal flow are presented in Figures 8. The Figure indicates that no sensible variation is predicted in longitudinal Mach number, especially in the inlet/converging part. The vertical line $x=x^*$ confirms that, for both cases, the Mach number value of unity is obtained at the critical cross section of the nozzle. This conclusion agreed very well with the predictions in recent studies (Arina, 2004, Molleson & Stasenko, 2005, and Drikakis & Tsangaris, 1993). It can, therefore, be concluded that the sonic position always occurs at the throat and is independent of the nozzle geometry and gas thermodynamic model.

**Shock position**: A shock wave occurs in the diffuser part of the system that leads to a change in the flow from supersonic to subsonic. The real gas model predicts the shock location earlier as concluded in Section 2.3.1. Arina (2004) compared several real gas EOS with the corresponding perfect gas model. He concluded that all the real gas models predict a similar flow in the convergent part, while the shock position is slightly varying from one model to another. However, his conclusion was built on a Laval nozzle and inert gases (air) which behave almost ideally even at high pressures. It can also be concluded that
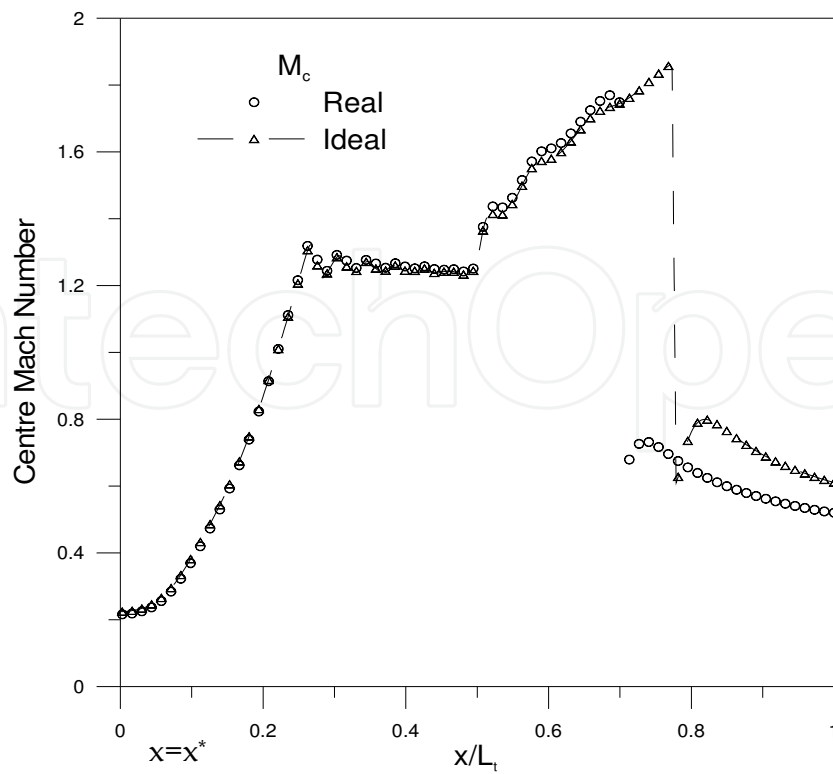
Fig. 8. Centerline Mach number for real vs. ideal methane simulation in an extended throat nozzle
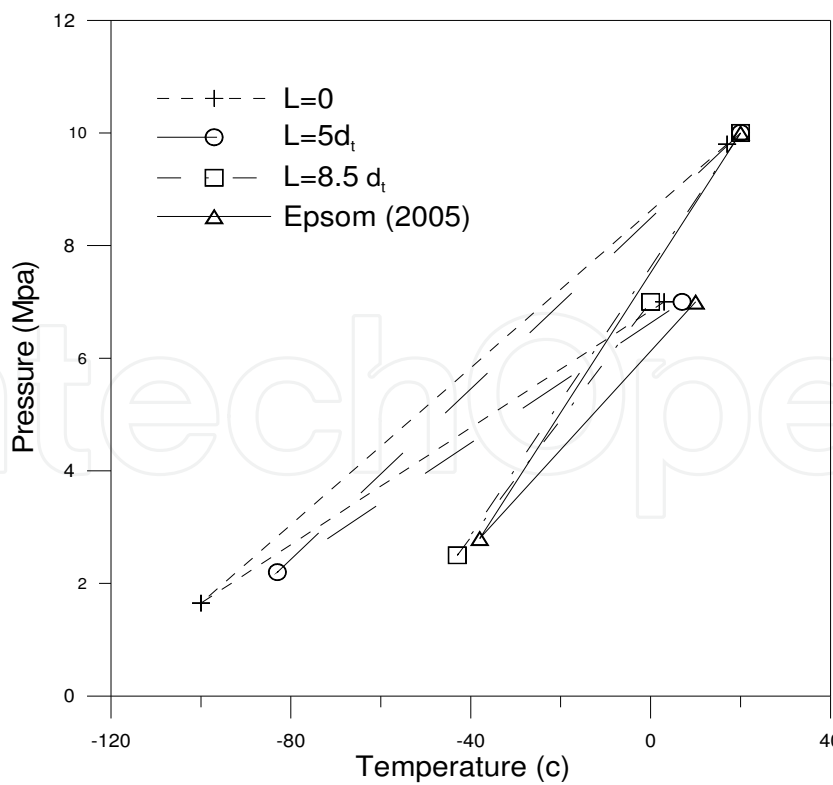


Fig. 9. Pressure-temperature chart for real gas (methane) simulation in an extended throat nozzle

thermodynamic models and the system's geometry play the most significant roles in predicting the shock position. Hence, the more accurate EOS would result in a closer prediction of the shock location and behaviour.

**Length of Constant Cross Section Area Conduit:** In order to separate liquid particles from natural gas and place instruments to control the shock wave location, Twister Inc. (Epsom, 2005) uses an extended constant area throat within the area just before the diffuser section of the Laval nozzle. Although the exact dimension and geometry of the Twister's nozzle are unknown, we studied the effect of the length of the constant cross section area conduit by selecting several length-to-diameter ($L/d_t$) ratios. The results of the simulation are plotted on a Pressure-Temperature (P-T) chart as shown in Figure 9. We could produce the same P-T chart as the Twister (Epsom, 2005) by changing the length of the conduit part by adjusting the ($L/d_t$) parameter. This indicates that, in addition to the nozzle outlet pressure, by adjusting the channel length, the minimum temperature of the system and shock position can be controlled.

## Mesh generation

The quality of the mesh plays a significant role in the accuracy and stability of the numerical computation. The issue of grid quality is concerned with the ability of a particular discretization scheme to accurately represent the continuous governing equations on a given grid. The final accuracy and efficiency of any numerical solution are highly dependent on the particular meshing strategies and the mesh density distribution employed. The key to an efficient overall numerical solution remains in a good matching of the strengths and weaknesses of the grid generation and flow solution techniques and the maintaining of a strong and favourable interplay between these two phases of the solution procedure. Obviously, the goal of any numerical simulation should be the optimization of both the discretization scheme as well as the grid generation scheme.

Although accuracy increases with finer grids, the CPU and memory requirements to compute the solution and post-process the results also increase. Of many solutions to such deficiency -adaptive grid refinement can be used to increase and/or decrease grid density based on the evolving flow field, and thus provides the potential for more economical use of grid points and hence reduced time and resource requirements. Multigrid strategy also represents another recent powerful technique which takes a more comprehensive approach to the general problem of numerically simulating a physical phenomenon by closely coupling the grid generation and numerical solution aspects. The idea of a Multigrid algorithm, which was considered in the present numerical technique, is to accelerate the convergence of a set of fine-grid discrete equations by computing corrections to these equations on a coarser grid (Peyret, 1996), where the computation can be performed more economically. This process is applied recursively to an entire set of coarse-grid levels. Each Multigrid cycle begins on the finest grid level and cycles through the various levels up to the coarsest mesh. At this stage the computed corrections are successively interpolated back to the finest level and the cycle is repeated. The accuracy of the final discretization is solely determined by the fine-grid discretization, and the coarser levels may be viewed simply as artefacts employed to accelerate convergence.

The dependence of the accuracy on the quality of the grid can be reduced if more grid metric information is included. However, grid dependency studies (Drikakis & Tsangaris, 1993) have shown that finer meshes do not necessarily influence the accuracy of the solution in the case of the axisymmetric nozzle flow. This conclusion was also reached in our

simulation when three different numbers of mesh cells, 1882, 5533 and 11 832 cells, were selected. Table 1 shows the number of iterations that led to convergence with respect to total mass error in inlet/outlet mass flow for each case. It is clearly shown that finer grid did not significantly affect the iteration steps for convergence. In fact, for coarser grids (i.e. 1882 cell), convergence occurred even faster (~1500 steps). However the position of shock changed and became stabilized after the number of iterations was doubled. The uncertainty of shock spot forces us to choose finer grids, especially since the shock wave is considered as one of the large gradient regions that requires grids to be fine enough to minimize the change in the flow variables from cell to cell. Due to the difficulties in determining the location of the shock in advance, one should strive to achieve a high-quality mesh over the entire flow domain. Hence, we considered 5533 grid cells as the computational mesh for the present study to endorse smooth variations of flow properties across shock region. Convergence occurred after a certain number of iteration steps and varied for real and ideal gas models. For example convergence for real gas non-swirl case occurred after 3182 iterations with an error in inlet/outlet mass flow of about $4.8 \times 10^{-4}$ %. Table 2 shows the number of iterations that led to convergence with residual errors for continuity, energy, $k$ and $\varepsilon$ equations for non-swirl real and ideal cases.

| No. of Cells | No. of Iterations | % errors in mass flow |
|---|---|---|
| 1 882 | 3 030 | $9.8 \times 10^{-3}$ |
| 5 533 | 3 182 | $4.8 \times 10^{-4}$ |
| 11 832 | 3 500 | $3.2 \times 10^{-1}$ |

Table 1. Number of iterations that led to convergence for simulation cases with total mass error in inlet and outlet mass flow

| Case | % Error of Inlet/Outlet Mass Balance | Number of Iteration Steps | Continuity | Energy | $k$ | $\varepsilon$ |
|---|---|---|---|---|---|---|
| Ideal | $2.0 \times 10^{-4}$ | 9 230 | $2.40 \times 10^{-3}$ | $1.90 \times 10^{-3}$ | $8.50 \times 10^{-6}$ | $9.60 \times 10^{-6}$ |
| Real | $4.8 \times 10^{-4}$ | 3 182 | $5.85 \times 10^{-4}$ | $5.58 \times 10^{-4}$ | $5.58 \times 10^{-5}$ | $6.03 \times 10^{-5}$ |

Table 2. Number of iterations that led to convergence with residual errors for continuity, energy, $k$ and $\varepsilon$ equations for non-swirl real and ideal cases

### 2.3.3 de Laval nozzles with extended U-shape throat

The purpose of this section is to find alternative designs to the swirling flow of gas through the Laval nozzle configuration that was discussed earlier in search of better separation performances. As a result, the Laval nozzle with extended U-shaped section was proposed. The proposed nozzle is composed of three sections:

1. The convergent subsonic section that experiences a slight divergence after the throat to accommodate for the supersonic flow of the gas.
2. The U-shaped extended throat through which the centrifugal force exerted on the particles is expected to provide the intended separation between phases (gas-liquid, gas-solid, or gas-solid-liquid).
3. The divergent section that provides the cross-sectional growth required for pressure recovery.

The design parameters in this study included the ratio of the inside diameter of the throat to that of the U-shaped section, the curvature radius of the U-shaped section, and the inlet and outlet pressures. System variables that were used in the analysis were position of the shock, gas velocity inside the U-shaped section, and consequently the centrifugal acceleration experienced by the gas flowing inside that section used as a measurement of the level of phase separation the device could deliver.

Simulations were based on the inviscid flow of methane as process fluid. The governing equations were those of the conservation laws (mass, momentum, and energy) along with an appropriate thermodynamic model to predict gas properties.

As no experimental results are available for evaluation purposes, a pilot test is under development that uses compressed air as process fluid. The test results will then be compared to those of the CFD simulations performed under the same conditions to evaluate the computer models.

### 2.3.3.1 Throat diameter ratio

As it was shown in the previous section, the flow always reaches sonic velocity at the throat. The slight divergence after the throat and before the U-shaped section is to allow the flow to reach supersonic velocity. Assuming pressure drop across the nozzle is large enough, the value of the Mach number at the entrance to the U-shaped section depends solely on the ratio of the diameter at this point to that of the throat. Since the purpose of the U-shaped section is to take advantage of the supersonic flow in a circular path, it is important that the shock takes place in the diverging section. It must be noted that despite the diameter of the nozzle is constant throughout the U-shaped section, a shock wave may take place inside that section due to the loss of energy in the U-shaped section.

The U-shaped section to throat diameter ratio of 1.2 was determined to be most effective in this study. This means that the constant cross-section area of the U-shaped section has a diameter of 1.2 times the diameter of the throat where the choke takes place. It is important to realize that this ratio is not the only factor that determines the position of the shock. Other parameters involved are the U-shaped section curvature radius and outlet back pressure.

### 2.3.3.2 U-shaped section curvature radius

The curvature radius of the U-shaped section has two converse effects on the flow. Increasing the radius of the curvature allows the gas to pass through it with faster velocity and higher Mach number without triggering a shock wave, but at the same time reduces the centrifugal acceleration (Bird, 1924). This is easily shown by the kinematic expression of tangential acceleration:

$$a_{\text{tangential}} = \frac{V^2}{r} \tag{4}$$

It may be concluded that since velocity is raised to the power of two in this equation, its value overweighs the negative value of increased radius. It should be noted though that an important feature of such supersonic separators is their relatively small size, and a rather large radius of curvature will compromise this characteristic. After vigilant study of several designs with various curvature radii, it was determined that a U-shaped section with a decreasing radius profile would be the best configuration for this design. The curvature profile shown in Figure 10 was therefore developed for the U-shaped section of the nozzle.

The radius of this profile is 40 units in the beginning (lower left section) and decreases continuously until it reaches 5 units in the end (upper section).
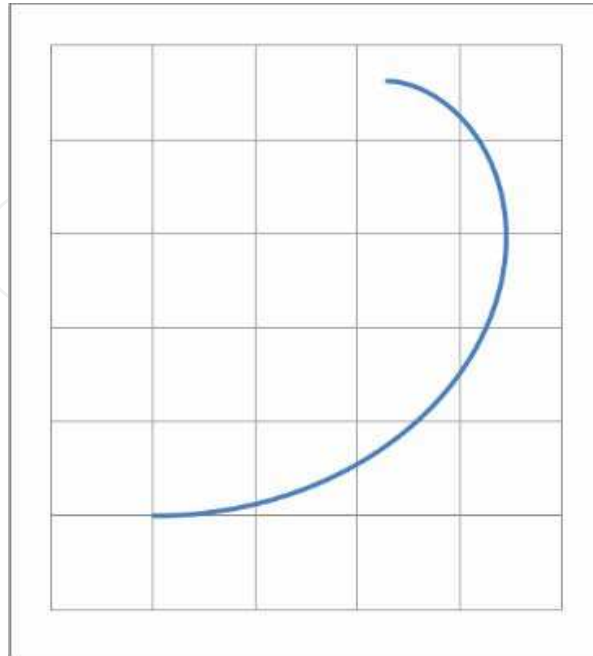


Fig. 10. A typical variable curvature proposed for the U-shaped section of the Laval nozzle.

2.3.3.3 Inlet pressure/Outlet back pressure

The outlet back pressure in this study was chosen to be the atmospheric pressure. The inlet pressure as well as the flow rate of the gas through the device were hence the other parameters affecting the pressure drop through the nozzle and consequently the position of the shock wave.

2.3.3.4 Particle Separation

Particle separation, as it was mentioned before, is due to the centrifugal force that is exerted on the flow as it passes through the U-shaped section with high velocity. The particles (e.g. micron size liquid droplets) are forced towards the outermost wall in the U-shaped section and may be extracted via a side channel that is installed in an appropriate position. Figure11 shows the values of centrifugal acceleration along this section as it is experienced by the flow. The acceleration is calculated from Equation (4). The graph is generated from the CFD simulation results for the geometry shown in Figure 12 when an inlet pressure of 345 kPa (50 psia) was imposed. It can be seen in the graph that the particles experience centrifugal accelerations of up to 36,000,000 m/s² in this particular configuration. That is the equivalent of approximately 3.7 million $g$.

2.3.3.5 Shockwave position

The position of the shockwave is very important for the performance of such separators. The shockwave should not take place before or through the U-shaped section as it was explained before. It is also important that the shock does not occur too far into the diverging section. This is because the farther into this section the shock takes place, it requires more differential pressure driving force across the device and therefore results in a greater pressure loss. It is crucial that the shock occurs as early as possible in the diverging section.
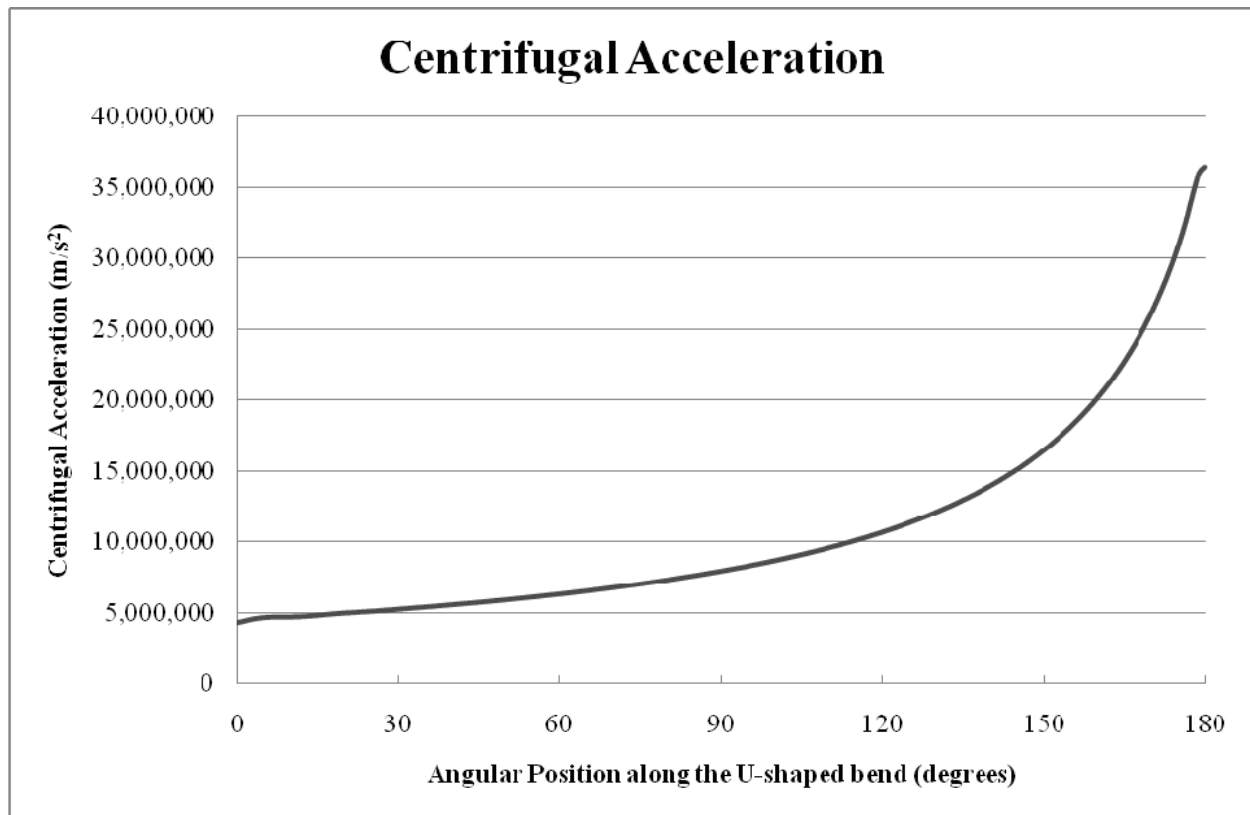
Fig. 11. Variation of centrifugal acceleration as a function of position along the U-shaped section in the proposed Laval nozzle.
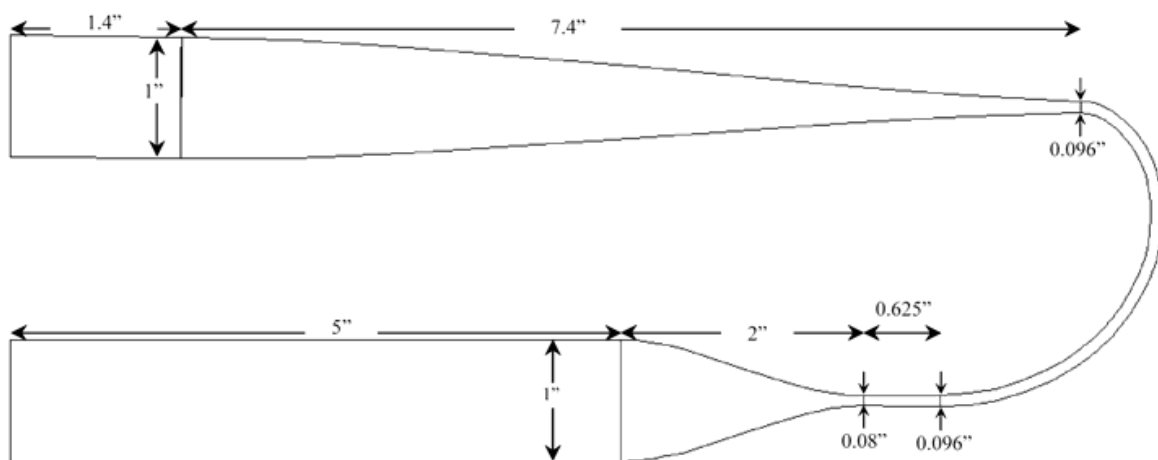


Fig. 12. A typical design configuration of the proposed Laval nozzle.

This property is one of the properties that were used to adjust the design and operating conditions of the separator. The position of the shockwave can be monitored through many different methods such as pressure profiling and velocity profiling. The most effective and accurate method that became available through the CFD package's post processing capabilities was the use of Mach number contours across the device. Theses contours clearly show the position of the shockwave as well as its shape and intensity (see Figure 13).
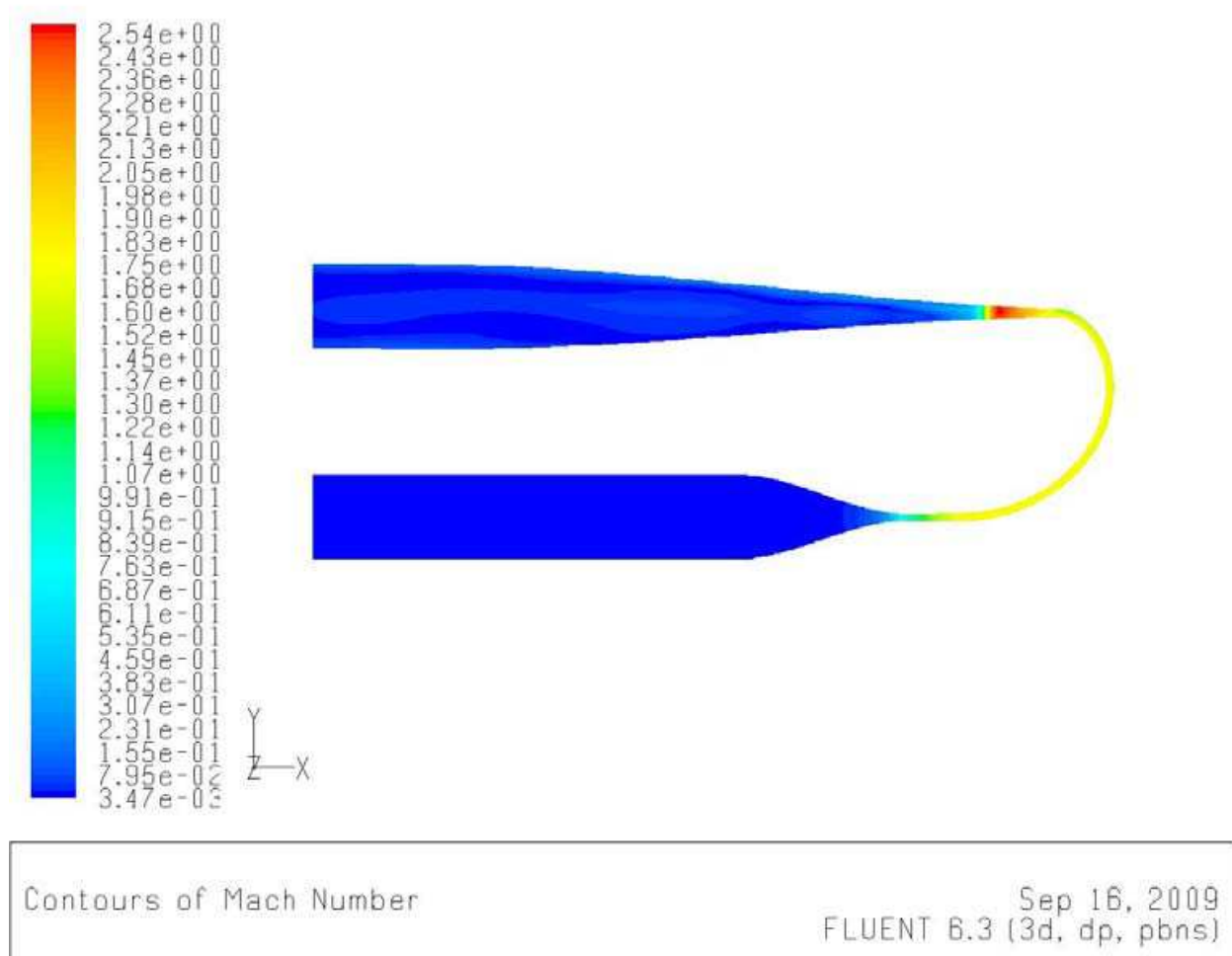
Fig. 13. Mach number filled contours showing the position of the shock wave.

2.3.3.6 Separation channel position

One important design parameter is to determine where the side channel to separate the flow of particles from the main gas flow should be placed. This can also be easily determined using the post processing features of the CFD package. Figure 14 is a volume density contour, precisely showing where most of the higher density particles are accumulated along the U-shaped section.

2.3.3.7 Mesh Generation

As it was mentioned previously, the quality of the mesh is a key factor in the accuracy and stability of a numerical (finite volume) analysis. Various characteristic properties of the geometry itself, types of fluids involved, and the amount of available memory and processing capability are some of the parameters that contribute to the final selection of a specific mesh design. A combination of wedge shaped and tetrahedral elements was chosen to represent the geometry in Figure 12. The geometry was divided into 6 sections as it can be seen in Figure 15. All sections were meshed using wedge shaped elements except section 2 which was meshed using tetrahedral elements due to the high gradient of cross-sectional area. Section 1 is only a simple pipe and its purpose is to stabilize the flow of gas before it enters the nozzle system. The meshing of this section therefore does not require a very fine quality. The mesh elements in this section are wedges with a length of $5.08 \times 10^{-3}$ m (0.2″) and

Contours of particles-volume-density (mixture)                    Jun 03, 2008
                                                                   FLUENT 6.3 (3d, dp, pbns, eulerian, rke)
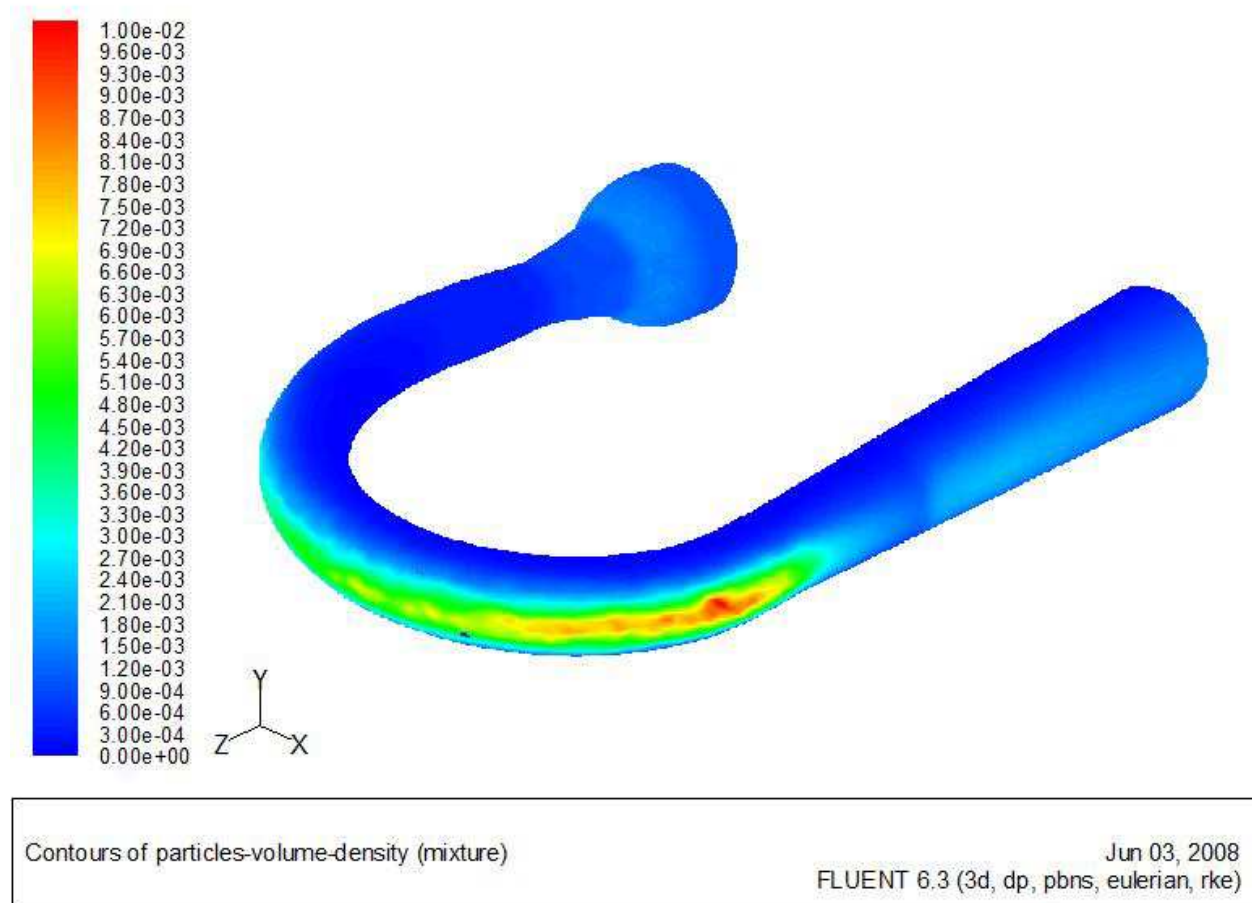
Fig. 14. A typical contour of the particles volume density showing where a side channel should be positioned to separate most of the particles
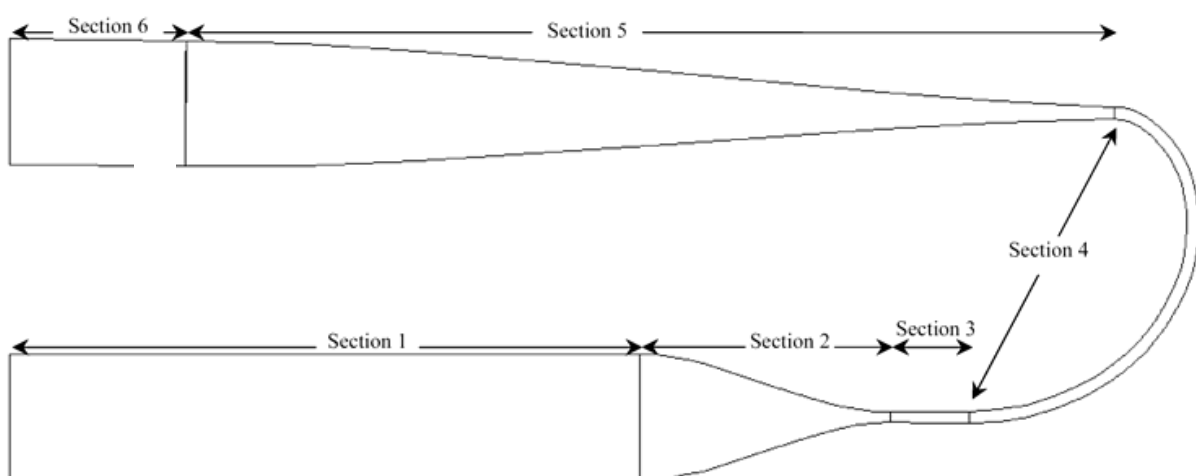


Fig. 15. Geometry divisions for meshing purposes.

equilateral triangular bases with edges of $2.54 \times 10^{-3}$ m (0.1″) (see Figure 16). Section 2 is the converging section of the nozzle and is meshed with a shrinking tetrahedral scheme (Figures 17 and 18). This method ensures the stability of the geometry through the

numerical analysis and links the coarse mesh of section 1 to the fine mesh of section 3. Section 3 is the slight divergence after the throat that accommodates for the supersonic flow of the gas and hence requires a very fine mesh quality to ensure the accuracy of the results. The meshing scheme is again a wedge type element that grows laterally as the cross section increases. The meshes are arranged so that there are 60 elements on the cross sectional perimeter at each point. This means that the wedge bases have lateral sizes of $1.016\times10^{-4}$ m (0.004″) in the beginning (right after the throat) and $1.27\times10^{-4}$ m (0.005″) in the end (right before the U-shaped section). A length of $2.54\times10^{-4}$ m (0.01″) is kept constant throughout this section. Section 4 is the U-shaped section. Wedge elements advance into this section with the same base sizes and lengths of $5.08\times10^{-4}$ m (0.02″). The wedges grow in section 5 until they reach a base size of $2.54\times10^{-3}$ m (0.1″) and length of $5.08\times10^{-3}$ m (0.2″) at the end of this section to merge in with section 6 that is the equivalent of section 1 and the mesh elements remain the same throughout this section. It is important to note that since the fluids being studied are gaseous and of high velocities, the effects of boundary layers may be neglected and hence no extra care is directed towards that area.
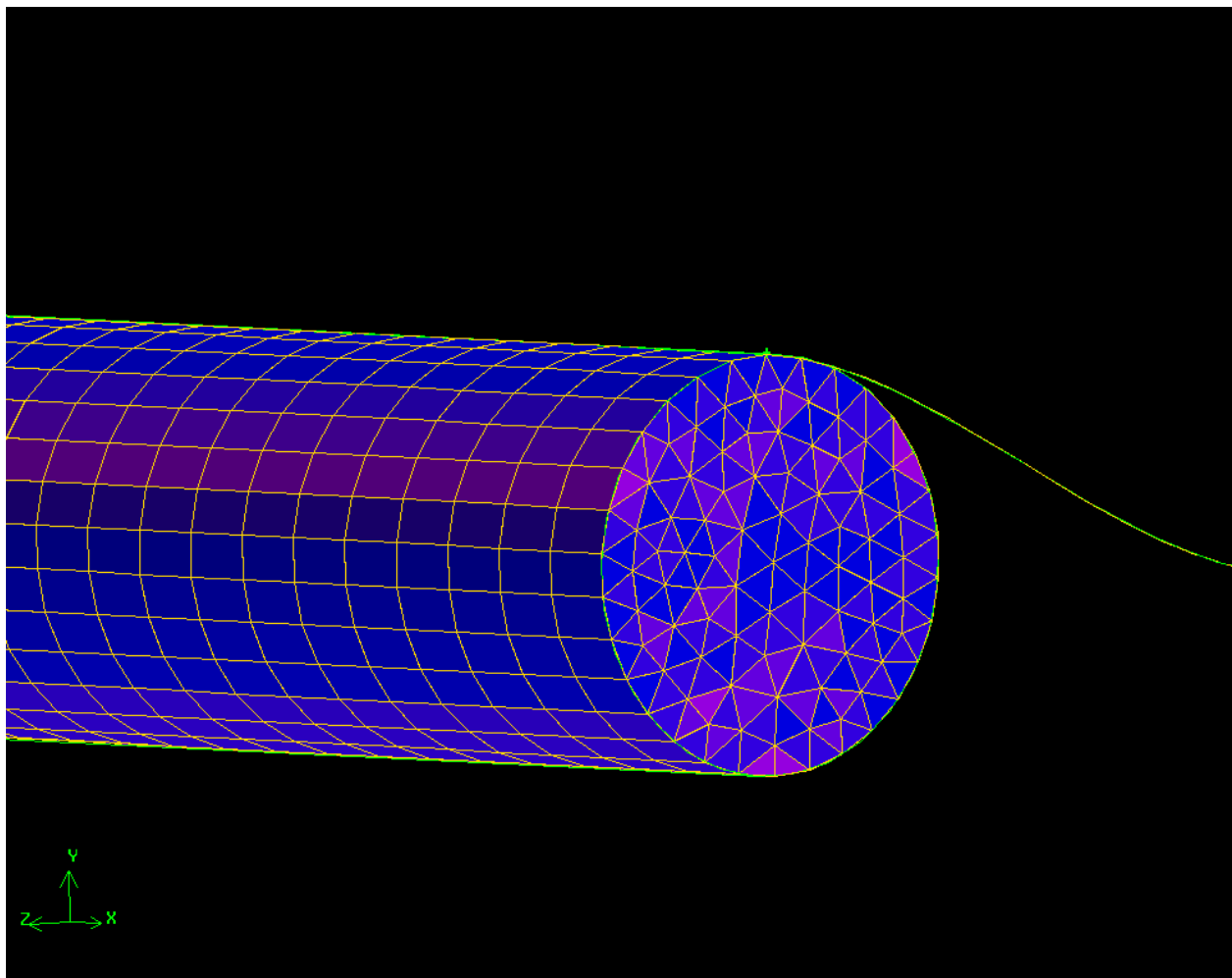


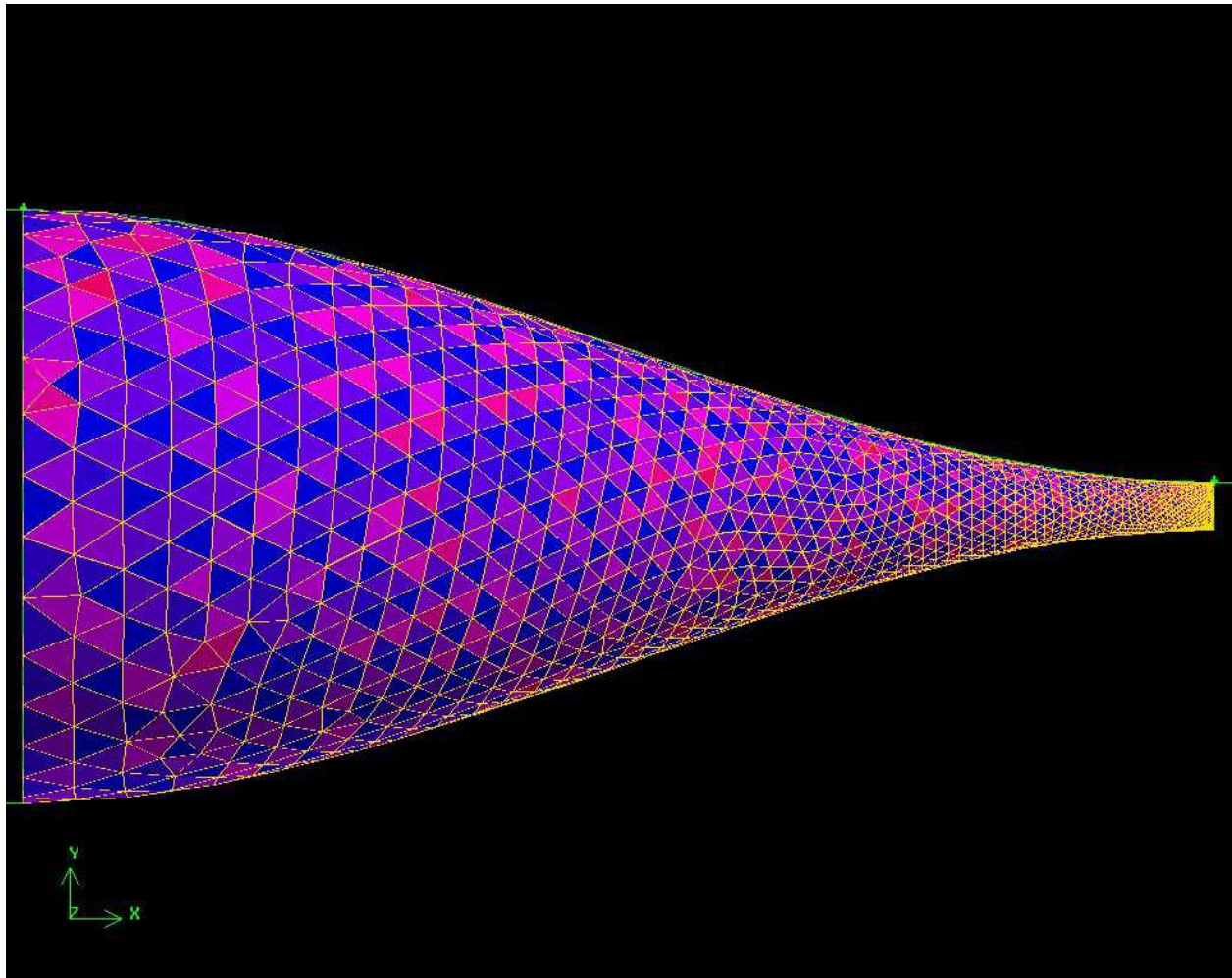Fig. 16. Wedge shaped mesh elements forming the inlet stabilizing section of the device (Section 1).

Fig. 17. Tetrahedral mesh elements in the converging section of the nozzle (Section 2). The element volumes shrink as they get closer to the throat.

2.3.3.8 Experimental apparatus

The novel nature of this study and the lack of external data inflicted the need to carry out laboratory pilot tests in order to evaluate the results of CFD simulations. The idea was to create a nozzle system similar to those that had been simulated through which high pressure gas would flow. Pressure, temperature, and flow rate measurements would be made and the results would be compared to those of the CFD simulations of the same system. The geometry chosen for this test was the geometry shown in Figure 12 and the process gas was compressed air. Two symmetrical halves of the proposed geometry was machined out of two blocks of aluminum and put together to form the desired pathways. Since it is significantly important that the flow is not disturbed by any bodily imperfection or hindrance, direct pressure and temperature measurement was not an option. Small size channels were created at several points along the pathway to enable the placement of measurement probes outside the fluid's pathway. As can be seen in Figure 19, there are 12 pressure measurement points and 4 temperature measurement points. Figure 20 shows the schematic setup of the pilot test. Measurements are currently being performed and the data is yet to be analyzed, but the preliminary results are in good agreement with the simulations.
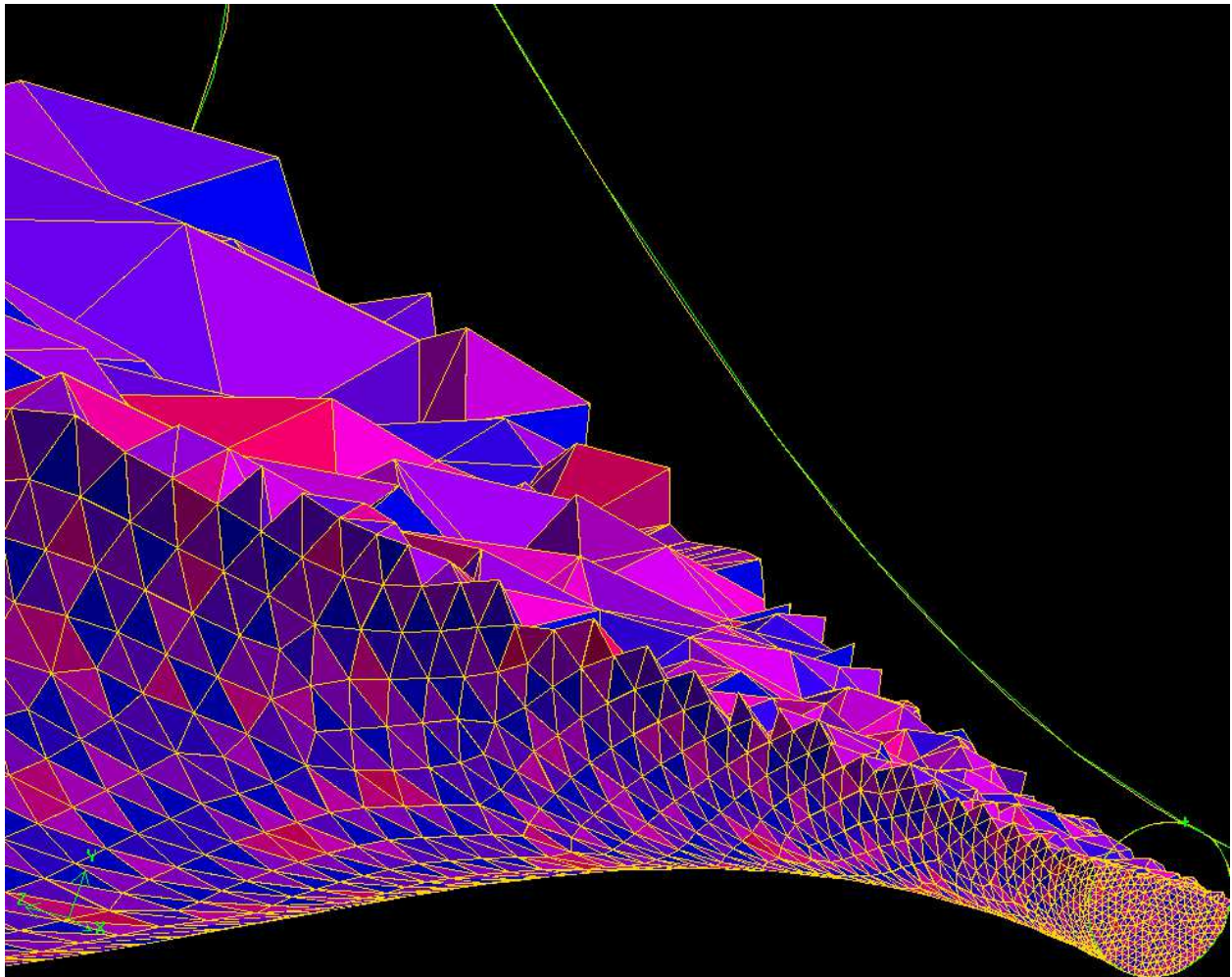
Fig. 18. A planar cut view of the mesh elements in the converging section of the nozzle (Section 2)

## 3. Cold jet release from high pressure marine CNG tanks

Cold jet is a result of a high pressure leak through a wall crack or valve stem or any other opening caused by an accident or failure to a high pressure device. Computational Fluid Dynamics, CFD, was used to study the phenomena and its effect on the surrounding equipment.

### 3.1 Problem description

The cold jet is developed when a fluid under high pressure and quite low temperature conditions is propelled to the ambient conditions through a crack or any leak opening. The very low temperature created due to this effect can influence the material's strength of construction of the high pressure containers/vessels or pipe systems carrying the gas. Very few studies have been conducted on this area while the demand is growing in the industry for such studies.

The low temperature can make ordinary carbon steel to become very brittle and lead to instant failure of high pressure tanks or pipelines and subsequent explosion. The jet can also extend to other adjacent equipment, parts, and pieces and influence their strength and
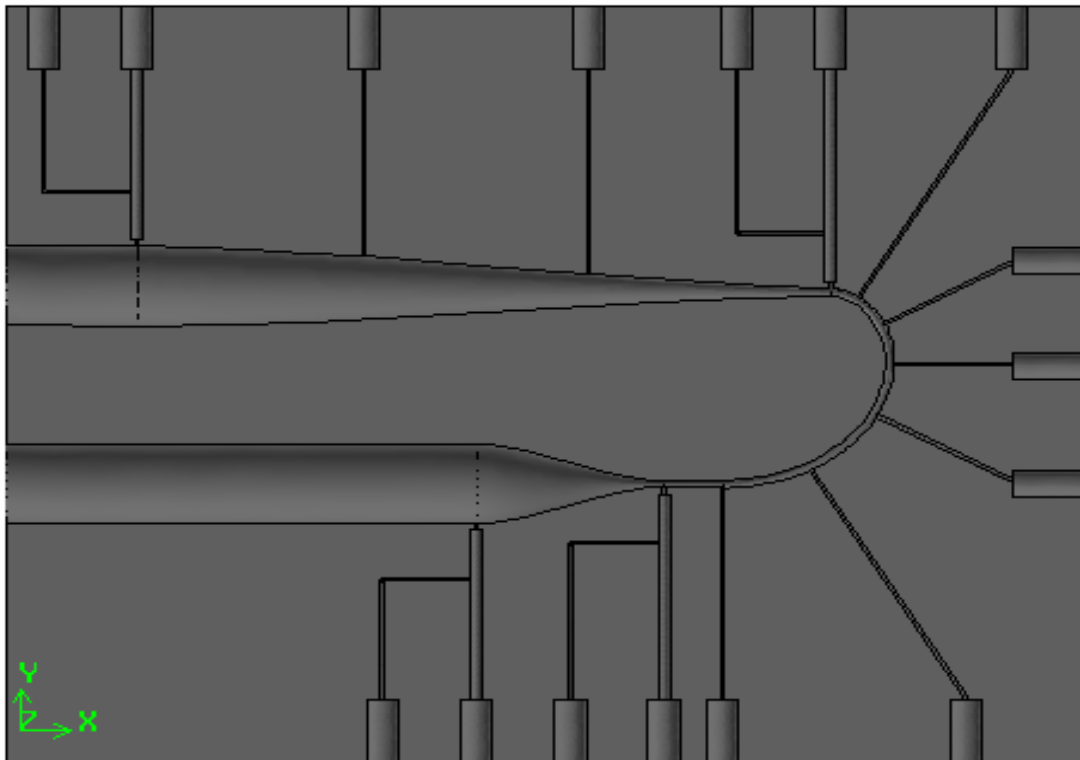
Fig. 19. The bottom piece of the pilot test nozzle system. The 4 thicker channels are designed to accommodate for temperature probes. All other channels are for pressure measurements.
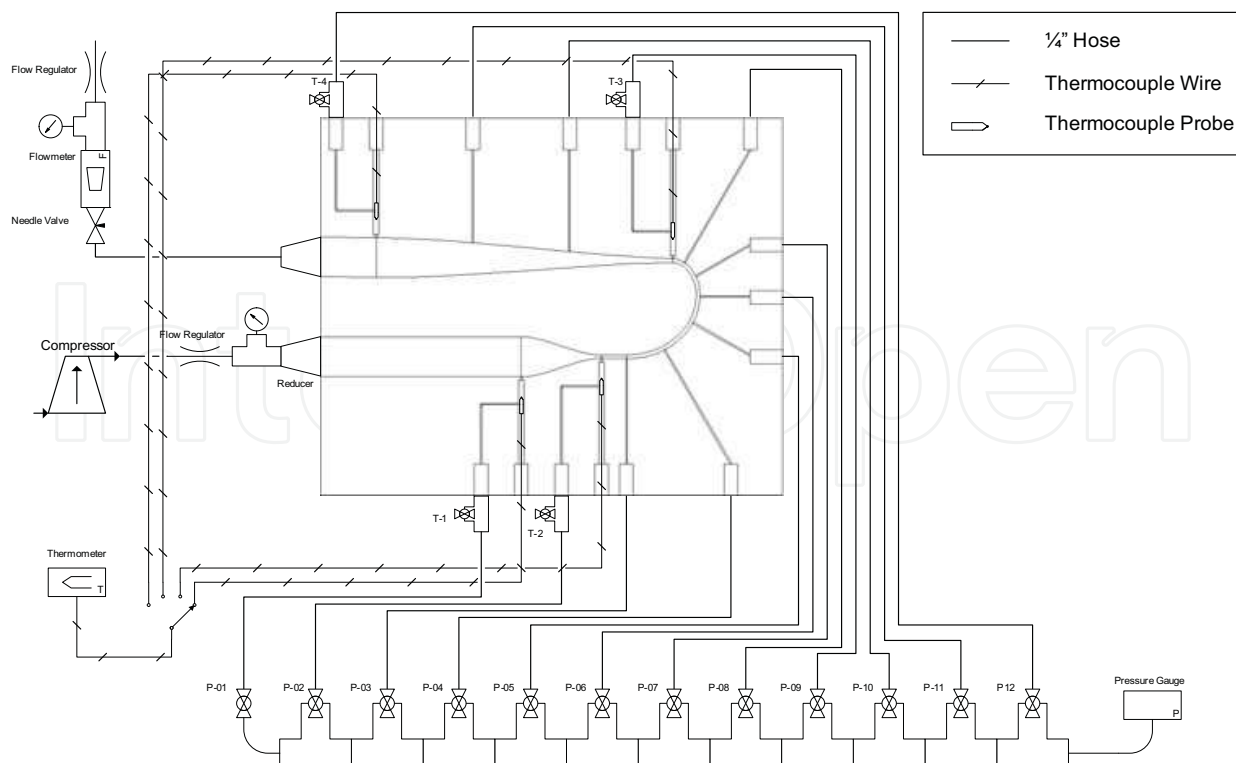


Fig. 20. Process flow diagram describing the schematic setup of the test pilot set-up

integrity due to temperature variations. The result of such study will provide an improved insight for any failure and stress analysis when such problems are encountered.

In this study, the behaviour of flow through the crack, the temperature distribution around the crack, and the influence of the jet to the adjacent walls have been reviewed.

The computational fluid dynamics technique was used to study the behaviour of high pressure natural gas when it flows through accidental cracks. The following themes are of interest in this study and will be discussed in this section:

- Flow behaviour through the crack
- Temperature distribution around the crack
- The influence of the jet to the adjacent walls

### 3.2 System configuration and simulation

The actual shape of the crack can be very irregular however for our analyses and to simplify the simulation a convergent nozzle with the geometry shown in Figure 21 was chosen. The conditions of the natural gas (methane) in the high pressure cylinders are: pressure 122 bars and temperature -8 ℃ (265K), the thickness of the cylinder was 19 mm.
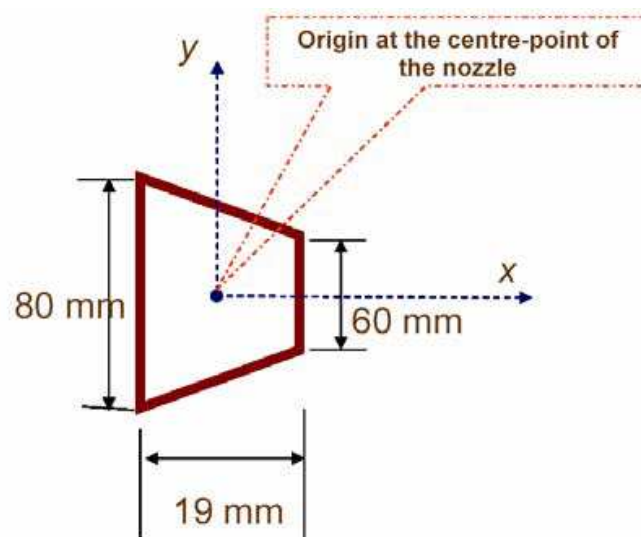


Fig. 21. Crack Geometry assumed to be convergent nozzle

### 3.3 Crack simulation and results

Figure 22 shows the Mach number variation along the crack wall. The choke flow conditions occur at the crack's exit point, which agrees well with the principles of thermodynamics. The distance is from the mid-point of the nozzle on the x-axis as seen in the Figure 21.

Wall static temperature variation shown in Figure 23 illustrates that the temperature decreases smoothly along the crack then declines very sharply near the exit, explaining the abrupt drop in pressure at crack exit.

### 3.3.1 Wall simulation around the crack

Temperature contours of the area around the crack can be generated by simulating the flow through the crack in a 2-D environment. Figure 24 shows the temperature contours on the outer wall surface of the tank at the crack exit. As can be seen the severe temperature differentials can pose thermal stress to the material and may cause fatigue and failure on the wall.
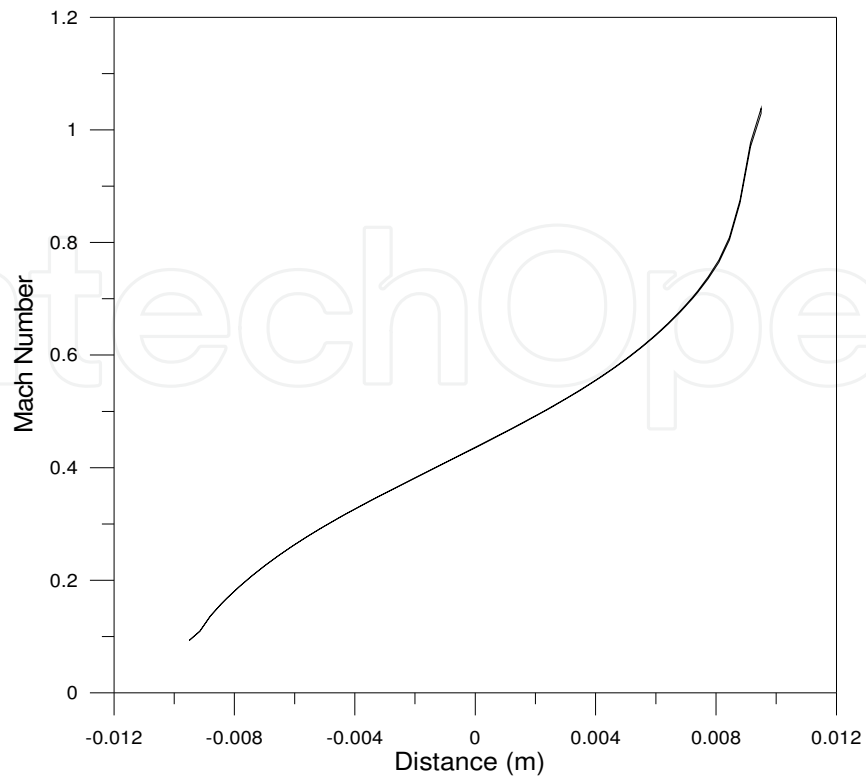
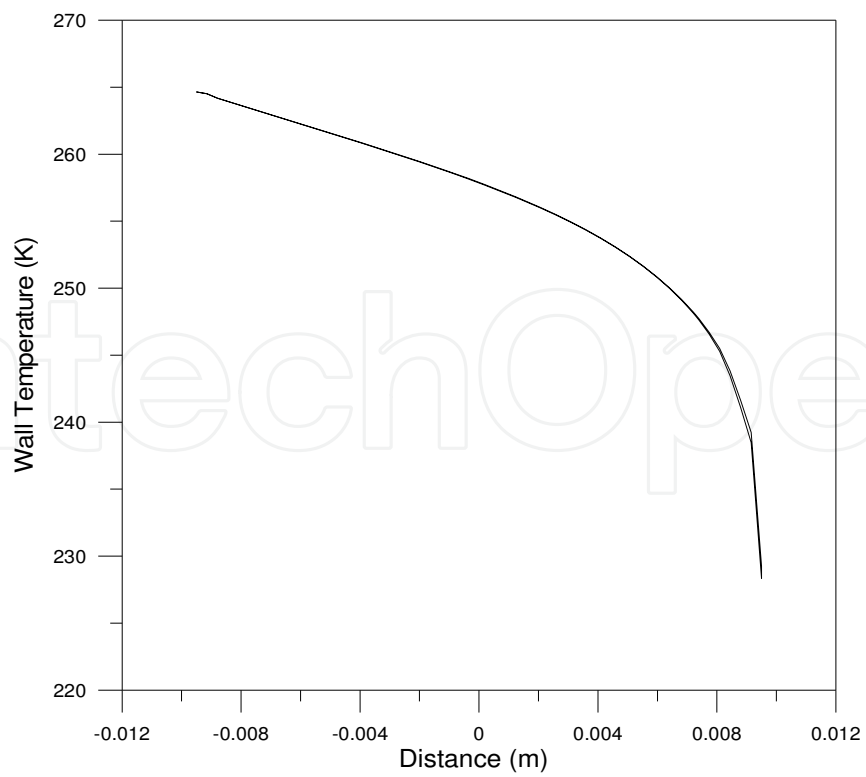Fig. 22. Flow Mach number at centerline of the Crack



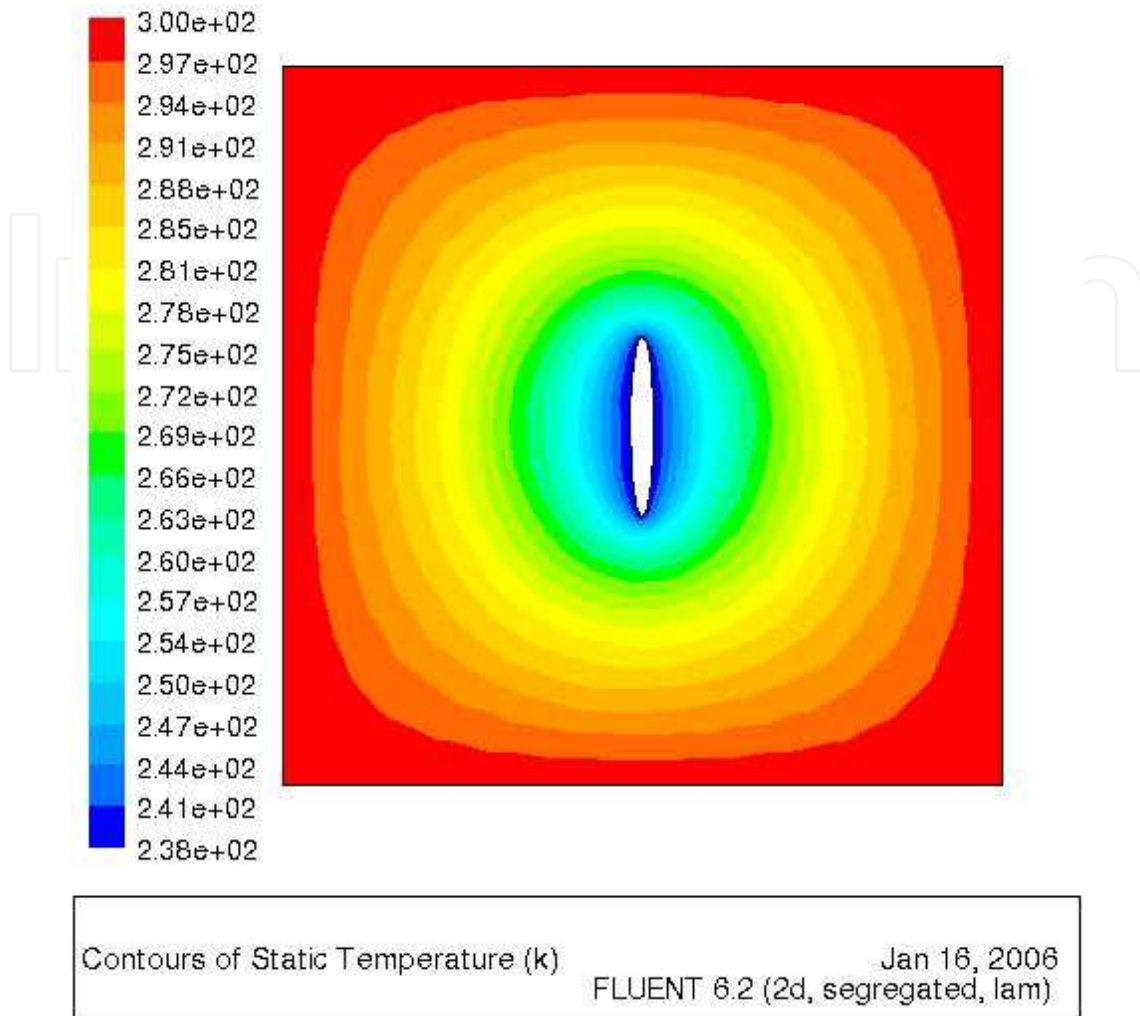Fig. 23. Temperature variation at the inner surface of the crack

Fig. 24. Temperature contours around the crack

**3.4 Jet simulation and results**

In this section, we simulated a jet of natural gas developing outside a tank hitting a stationary wall some distant apart. Jet velocity contours are shown in Figure 25. One can recognize the impinging region and how the flow direction changes because of stagnation spot. The altered stream strikes the wall of the adjacent components (here another tank with the same height) and leaves a certain area that is exposed to impingement under less strength. Thus the temperature of this area becomes relatively higher.

It is concluded from the simulation that temperature distribution along the adjacent wall can be divided into three regions, Figures (26a, 26b):
1.   Impinging point vicinity
2.   Sharp variation region
3.   Mild variation region

As seen in the jet velocity profile near the adjacent wall in Figure 25, the flow slightly alters then severely changes its direction to become parallel to the wall as it moves closer. Thus there is a certain distance on the wall that stagnation or circulated flow (eddies) are in contact with the wall. Hence the temperature of this region decreases sharply from a certain value (at stagnation spot) then increases gently along the rest of distance on the wall.
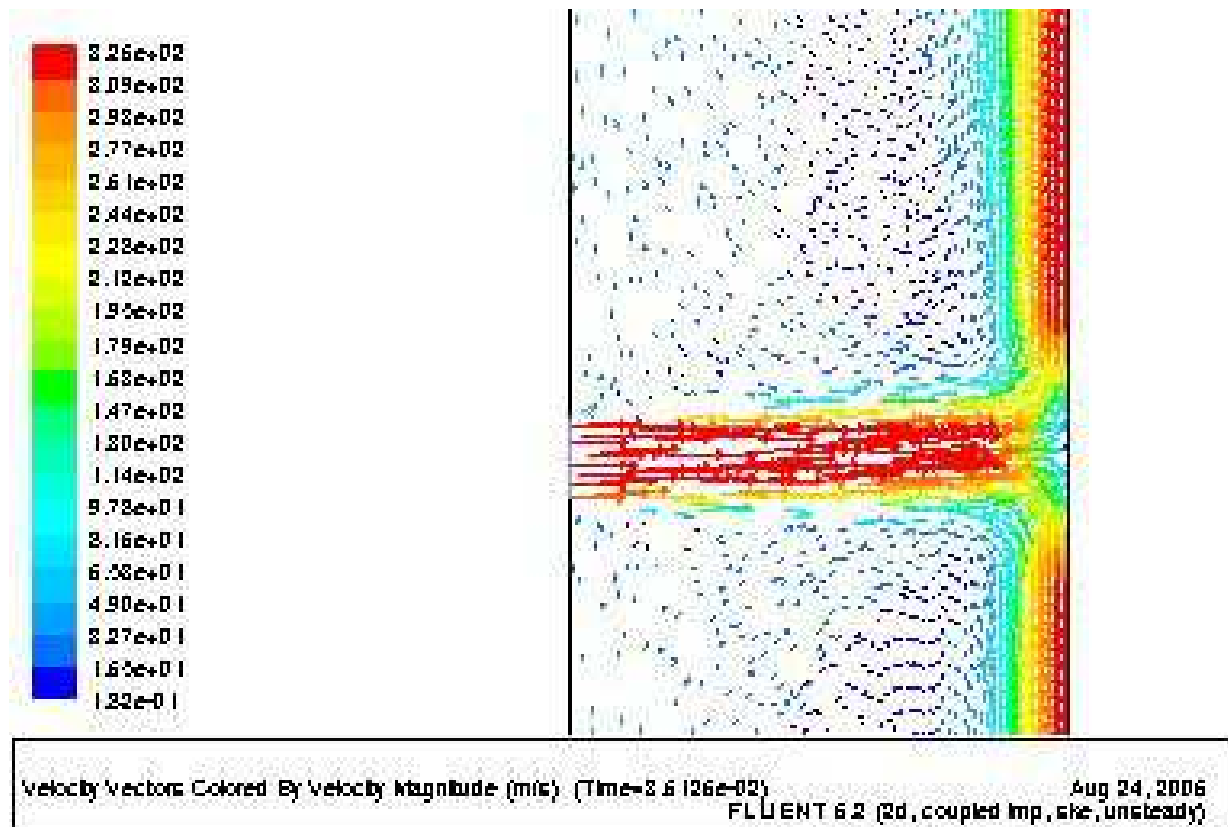
Fig. 25. Jet velocity vector caused by impinging with adjacent wall

## 4. Conclusions

Main conclusions can be summarized as follows:

- Shockwave has been studied using the CFD approach. The effects of real gas properties on the flow behavior were also addressed. It is crucial to beware of the real gas fluid behavior when analyzing high pressure natural gas flow systems. The assumption of a perfect gas may give rise to significant errors. Comparison between perfect and real gas models was implemented to present the errors involved when real properties in calculating heat, work, and other thermal processes are ignored. The results of CFD simulation runs conducted for different gases showed that the ideal gas assumption would lead to serious misrepresentation of the flow field, including the position of shockwave and severe miscalculations in the design of supersonic devices.

    The influence of geometry and vorticity were studied. Since the addition of a channel within the Laval nozzle is of interest in separating liquid particles, various lengths of such extended constant area regions, which connect the nozzle part with the diffuser part, have been selected. Results showed that variation of the channel length would impact the position of the shock wave and the minimum temperature of the system, which in turn influence the quantity and quality of droplets if condensation occurs. Swirls are formed when the fluid enters the nozzle semi-tangentially. Strength of vorticity and its behavior were addressed because the centrifugal force is responsible for particle separation due to the very high centrifugal acceleration induced within the nozzle throat. This acceleration is in the order of 105 or 106 times the acceleration of
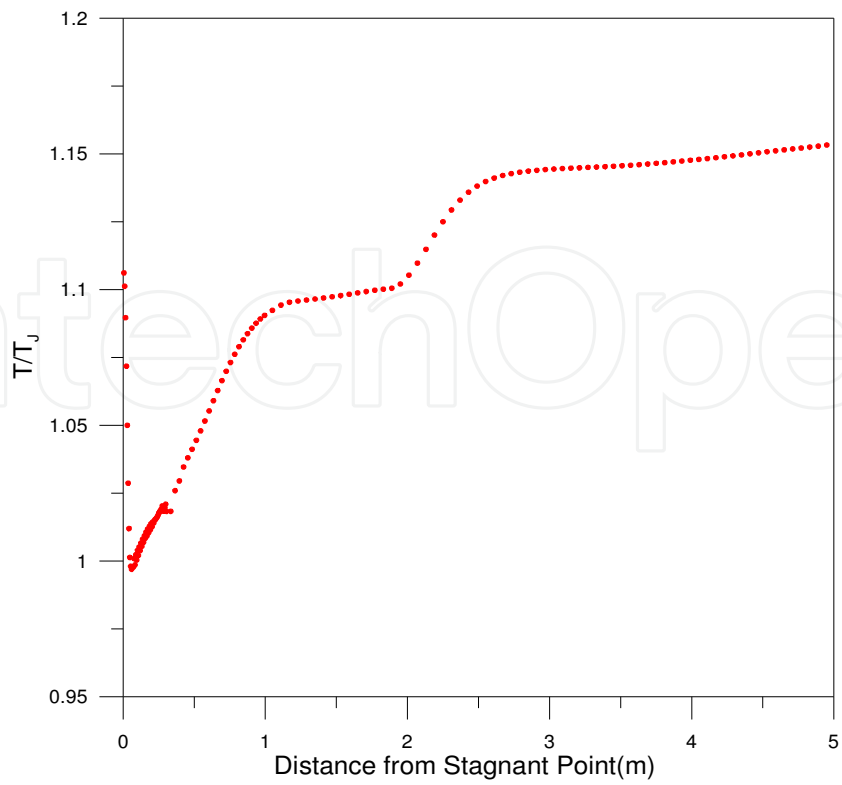
(a)
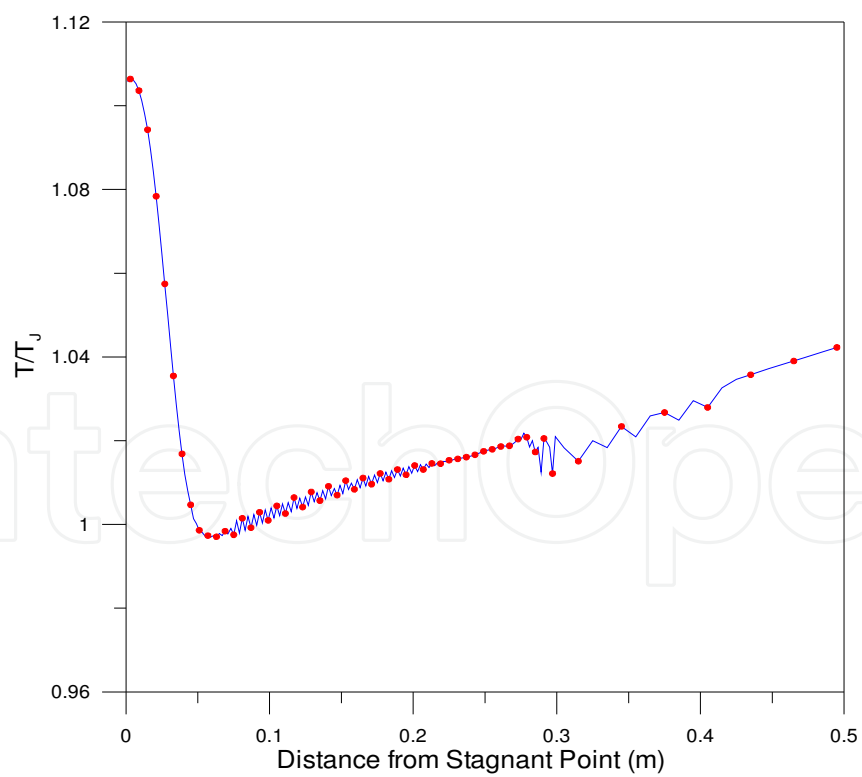


(b)

Fig. 26. Wall temperature ratio as a function of distance from stagnant point: a. Temperature profile at the adjacent wall; b. Enlarged portion wall temperature profile at the stagnant region

gravity and can induce separation of particles as small as several tenths of a macron in diameter. Furthermore, it is very important to have a sound understanding of pressure losses across the system, as these losses influence the economy of supersonic nozzles in natural gas processing. as the loss of pressure has to be compensated by costly compression facilities. In our further work, we will include the multiphase as well as multi-component fluid systems where the behavior of the natural gas in the system can be analyzed with more accuracy.

- It is concluded at this point that the alternate configuration of nozzle with an extended U-shaped section can deliver better separation performances than the original swirling flow of gas in a straight nozzle. Although the centrifugal acceleration levels observed here are highly dependent on the geometry size (curvature radius), it can be speculated that very powerful centrifugal forces can be achieved in a full size separator of this type. Despite the lack of external data, the CFD simulations have proven to be significantly reliable. The practical application of this system may look far away, but the use of CFD simulations has shown great potential and encouraging results.

CFD simulation is a very efficient technique to study the flow of high pressure gas through complex geometries and sophisticated simulations such as impinging region. This study showed how CFD could be used in analyzing such phenomena with elucidation that gives it a robust position among other algorithms. The selection of the right thermodynamic model is very crucial in simulating natural gas flow under high pressure and low temperature conditions. Results show that divergent geometry of the crack changes the flow from subsonic to supersonic flow. Hence, irreversibility is clearly affecting the properties of the flow through the crack. CFD simulation for cold jet concluded that adjacent components will be affected by the jet. The temperature varies according to the impinging phenomena in both shapes, however the temperature difference between the jet and adjacent wall is relatively higher in divergent shape than convergent. Further, heat exchange due to collision of jet with the adjacent storage tanks shows significant effects on the temperature distribution.

## 5. Acknowledgement

## 6. References

Alfyorov, V., Bagirov, L., Dmitriev, L., Feygin, V., Imayev S., Lacey, J. R., 2005. Supersonic Nozzle Efficiently Separates Natural Gas Components. Oil and Gas Journal. 103(20), 53-58.

Arina R., 2004. Numerical Simulation of Near-Critical Fluids. Applied Numerical Mathematics 51(4), 409-426.

Bai-Shi-I, 1961. An Introduction into Theory of Compressible Liquid Flow, Moscow: Izd. Inostrannoi Literatury, (Russ. Transl.)

Bird, R.B., 1924. Transport Phenomena. John Wiley & Sons, New York; USA.

Brouwer, J.M., Epsom, H. D., 2003.  Twister Supersonic Gas Conditioning for Unmanned Platforms and Sub sea Gas Processing Source. Offshore Europe Conference - Proceedings, Aberdeen, UK, pp. 219-225.

Carvero, C., and Satta, A., 2000.  A CFD Model for Real Gas Flow. ASME paper, GT-518.

Crocko, L., 1950. One-Dimensional Consideration of the Gas Dynamics of Time-Independent Flows, in Fundamentals of Gas Dynamics, H.W. Emmons, Ed., Princeton: Princeton University Press, Princeton, USA.

Drikakis, D., Tsangaris, S., 1993. Real Gas Effect for Compressible Nozzle Flows. Journal of Fluid Engineering. 115(117), 115-120.

Ginzburg, I. P., 1939. Uch. Zap. Leningr. Gos. University, no. 42, pp. 5.

Hengwei, L., Zhonggliang, L., Yongxun, F., Keyu, G., and Tingmin,Y., 2005.  Characteristic of a Supersonic Swirling Dehydration System of Natural Gas. Chinese Journal of Chemical Eng., 13(1), 9-12.

Kouremenos, D. A., 1986. Normal Shockwaves of Real Gases and the Generalized Isentropic Exponent. Forschung im Ingenieurwesen, 52(1), 23-31.

Karimi, A., and Abedinzadegan Abdi, M., 2006. Selective Removal of Water from Supercritical Natural Gas. SPE 100442, Proceedings of the SPE Gas Technology Symposium, Calgary, Alberta, Canada, 15-18.

Man, H. C., Duan, J., Yue, T. M., 1997.  Design and Characteristic Analysis of Supersonic Nozzle for   High Pressure Laser Cutting. Journal of Materials Processing Technology, 63(1-3), 217-222.

Molleson, G.V. and Stasenko, A. L., 2005.  An Axisymmetric Flow of a Mixture of Real Gases with a Condensing Component. High Temperature, 43(3), 422-430.

Okimoto, F., Brouwer, J. M., 2002. Supersonic Gas Conditioning. World Oil, 223(8),  89-91.

Peng, D. Y., and Robinson, D. B., 1976.  A New Two-Constant Equation of State. Ind. Eng. Chem. Fundam., 15, 59-64.

Pope, S. B., 2000.  Turbulent Flows. Cambridge University Press. Cambridge, USA.

Redlich, O., and Kwong, J. N. S., 1949.  On the Thermodynamics of Solutions. V. An Equation of State. Fugacities of Gaseous Solutions. Chem. Rev., 44, 233-244.

Saad M. A., 1993. Compressible Fluid Flow. 2nd Edition, Prentice-Hall, Inc., New Jersey, USA.

Soave, G., 1972.  Equilibrium Constants from a Modified Redlich-Kwong Equation of State. Chemical Engineering Science, 27(6), 1197-1203.

Wark, K., 1995.  Advanced Thermodynamics for Engineers. McGraw-Hill Series, New York, USA
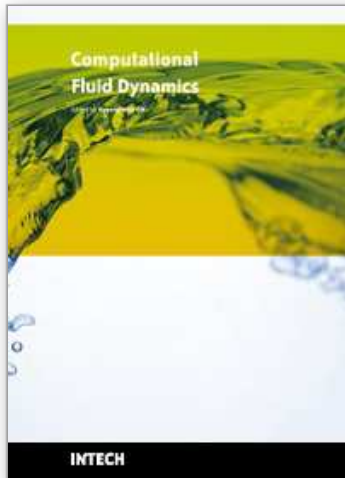
**Computational Fluid Dynamics**

Edited by Hyoung Woo Oh

ISBN 978-953-7619-59-6

Hard cover, 420 pages

**Publisher** InTech

**Published online** 01, January, 2010

**Published in print edition** January, 2010

This book is intended to serve as a reference text for advanced scientists and research engineers to solve a variety of fluid flow problems using computational fluid dynamics (CFD). Each chapter arises from a collection of research papers and discussions contributed by the practiced experts in the field of fluid mechanics. This material has encompassed a wide range of CFD applications concerning computational scheme, turbulence modeling and its simulation, multiphase flow modeling, unsteady-flow computation, and industrial applications of CFD.

**How to reference**

In order to correctly reference this scholarly work, feel free to copy and paste the following:

Majid Abedinzadegan Abdi, Esam Jassim, Mohammad Haghighi and Yuri Muzychka (2010). Applications of CFD in Natural Gas Processing and Transportation, Computational Fluid Dynamics, Hyoung Woo Oh (Ed.), ISBN: 978-953-7619-59-6, InTech, Available from: http://www.intechopen.com/books/computational-fluid-dynamics/applications-of-cfd-in-natural-gas-processing-and-transportation

# INTECH
open science | open minds